J. Fluid Mech. (1979), *vol.* 92, *part* 1, *pp.* 53–96
Printed in Great Britain

Gravity flow of cohesionless granular materials in chutes and channels

By STUART B. SAVAGE

Department of Civil Engineering and Applied Mechanics,
McGill University, Montreal, Canada

(Received 4 May 1977 and in revised form 13 April 1978)

A constitutive equation appropriate for flow of cohesionless granular materials at high deformation rates and low stress levels is proposed. It consists of an extension and a reinterpretation of the theory of Goodman & Cowin (1972), and accounts for the non-Newtonian nature of the flow as evidenced by Bagnold's (1954) experiments. The theory is applied to analyses of gravity flows in inclined chutes and vertical channels. Experiments were set up in an attempt to generate two-dimensional shear flows corresponding to these analyses. Velocity profiles measured by a technique which makes use of fibre optic probes agree qualitatively with the theoretical predictions, but direct comparison is inappropriate because of unavoidable side-wall friction effects in the experiments. The existing measure of agreement suggests that the most prominent effects have been included in the proposed constitutive relations. Tests in the inclined chute revealed the possible existence of surge waves and granular jumps analogous to hydraulic jumps.

CONTENTS

0022–1120/79/4097–5230 $02.00

1. Introduction

The mechanics of the flow of granular materials or bulk solids† such as sands, powders, seeds and grains is poorly understood at the present time. Relatively few fundamental studies of such flows have been performed despite the fact that there are numerous applications in mineral processing and many chemical and pharmaceutical industries. A basic understanding of the flow mechanics would be extremely useful, for example, in the design and operation of material handling equipment such as bins and hoppers, chutes, channels, conveyors and mixers.

The most commonplace and probably the earliest application of flow of granular materials is the hour-glass; it came into use in the early 14th century for measuring the speed of ships and continues today as the humble egg-timer. Although some early investigations of granular materials were conducted by Hagen (1852), who studied the flow of sand in tubes, and by Reynolds (1885), who formulated the idea of dilatancy (the expansion of a closely packed assemblage of solid particles when the bulk is deformed), little further work was done until more recent times. Reviews of the flow of bulk solids may be found in the article by Wieghardt (1975), the book by Brown & Richards (1970) and a report of a Working Party of the Institution of Chemical Engineers (Richards 1966). Many of the problems mentioned therein are quite complex and likely to embrace aspects of traditional fluid mechanics, plasticity theory, soil mechanics and rheology. Valentin has declared, perhaps rather boldly, that the study of bulk solids is 'one of the few remaining new frontiers in engineering' (see forward to Richards 1966).

1.1. *Previous work on quasi-static flows*

Much of the previous work on granular flows has dealt with confined flow in bins and hoppers (some typical recent examples are Bransby & Blair-Fish 1974, 1975*a*, *b*; Lee, Cowin & Templeton 1974). For the most part, this work dealt with situations or flow regions where the inertia effects associated with both the individual particle interactions and the bulk deformations are negligible. The emphasis has been on the visualization of the flow patterns, either by using dyed particles (e.g. Gardner 1966) or by X-ray techniques (e.g. Blair-Fish & Bransby 1973; Lee *et al.* 1974), and the measurement and prediction of wall stresses (e.g. Perry & Jangda 1970; Bransby &

† We define a bulk solid as an assembly of discrete solid components dispersed in a fluid such that the solid constituents are in contact with near neighbours. The solid phase is dominant and the material's behaviour is governed by interparticle cohesion, friction and collisions.

Blair-Fish 1974; Savage & Yong 1970; Jenike, Johanson & Carson 1973). The motivations have been the need for bin and hopper shapes which permit the bulk solid to flow freely without stoppage and the need to devise rational methods for prediction of wall stresses to avoid failures that sometimes have occurred in the past (Theimer 1969).

Typically, predictions of the stress fields have been obtained by solving the quasi-static equilibrium equations under the assumption that the bulk solid obeys the Coulomb yield or failure criterion in accordance with the Mohr–Coulomb theory of limiting equilibrium (Sokolovski 1965). Yielding is influenced by hydrostatic pressure in the Coulomb failure criterion, which states that yielding will occur at a point on a plane element when

$$|S| = c + T\tan\phi, \tag{1.1}$$

where S and T are respectively the shear stress and normal stress acting on the element, c is the cohesion and ϕ is the internal angle of friction of the bulk solid. While the above approach has commonly been applied, none the less uncertainty does exist about the general validity of the Mohr–Coulomb criterion, particularly about the choice of ϕ. It is usual to take ϕ as constant for the mass of granular material although it is well known to be dependent upon the strain (Roscoe 1970) and thus upon the fractional solids content ν, the volume of solids per unit bulk volume (in soil-mechanics terminology ν equals one minus the porosity).

The uncertainties mentioned are relatively minor when compared with those associated with the constitutive equation relating stresses and strain rates that one requires for the prediction of the velocity field during flow of granular materials. Several quite different analyses which attempt to formulate equations to describe the velocity field exist in the soil-mechanics literature (among them are Drucker & Prager 1952; Geniev 1958; de Josselin de Jong 1959, 1971; Takagi 1962; Spencer 1964; Zagaynov 1967; Mandl & Fernández-Luque 1970; James & Bransby 1971). None of these theories, most of which have been reviewed by Mandl & Fernández-Luque (1970), are universally or even widely accepted. In extensive passive earth pressure tests (Roscoe 1970) as well as studies of initial deformations of sand in mass flow bunkers (Bransby & Blair-Fish 1975*a*, *b*) using radiography, the Cambridge Soil Mechanics Group has observed that the rupture surfaces coincide with the lines of zero extension. They have discussed cohesionless materials in which ϕ is different from the angle of dilation δ. Assuming Saint-Venant's hypothesis that the principal axes of stress and strain rate coincide, the velocity characteristics (which correspond to the zero-extension lines) make angles of $\frac{1}{4}\pi - \frac{1}{2}\delta$ to the direction of the major principal stress whereas the stress characteristics are inclined at $\frac{1}{4}\pi - \frac{1}{2}\phi$. Most of the earlier analyses by others differ considerably from this approach. For example, Geniev (1958) assumes the material to be incompressible ($\delta = 0$) and that the principal axes of the strain rate are inclined at $\pm\frac{1}{2}\phi$ to the principal axes of stress, in violation of Saint Venant's hypothesis. Takagi (1962) permits the material to expand or contract during deformation but proposes that the stress and strain-rate *characteristics* coincide. De Josselin de Jong (1959, 1971), Mandl & Fernández-Luque (1970) and Spencer (1964) assume that the material is incompressible and deforms in plane strain by shear along the stress characteristics. These three analyses show that the principal axes of the stress and strain rate need not coincide but may be inclined at any angle between $\pm\frac{1}{2}\phi$. However, the constitutive relations are different; Spencer's

relation satisfies the principle of material-frame indifference whereas the relation of Mandl & Fernández-Luque is not independent of a superimposed uniform rigid-body translational motion (Spencer 1971). It would not be unfair to say that all of the above analyses are contentious to some degree in the soil-mechanics context (see papers and discussion of Session 2 of the Roscoe Memorial Symposium, Parry 1971) and that the applicability of any of them to continuous flow of bulk solids is uncertain.

1.2. *Flows where inertia and/or strain-rate effects are important*

Most of the above-mentioned analyses were intended for slow yielding or flow of granular materials; the stress components were determined by use of a yield criterion and the equilibrium equations (neglecting the inertia forces). The kinematics of the flow field were related to the previously determined stress field. The magnitudes of the stress components were assumed to be unaffected by the rates of deformation. While this assumption may be appropriate to some very slow granular flows, for example in the upper parts of bins and hoppers, there are other instances, such as gravity flow in chutes and pipes, where inertia and strain-rate effects are likely to be important. In these faster shear flows, as well as in the slower 'quasi-static' flows, one of the central theoretical problems is the development of constitutive equations that can be used for the prediction of flows in various practical devices.

The flow rate of granular materials from hoppers has been the subject of several experimental studies (see Brown & Richards 1970, chap. 6) and a few analyses (Brown 1961; Savage 1965, 1967; Davidson & Nedderman 1973). Although the consideration of inertia forces played an essential role in all of these analyses, the analyses were simple, approximate ones which neglected the details of the velocity profiles and did not require the use of a constitutive equation relating stresses and strain rates in order to predict overall flow rates.

A few experimental investigations of the flow of bulk solids in pipes and chutes have been conducted. Some had specific technological applications in mind (e.g. Wolf & Von Hohenleiten 1945; Choda & Willis 1967) while others were aimed more towards obtaining a better understanding of the flow mechanics. Bingham & Wikoff (1931) measured the gravity flow of dry sand through circular glass tubes of small diameter and found the surprising result that the mass flow rate increased with tube length. Richards (see Brown & Richards 1970, p. 185) has obtained similar results. The phenomenon is no doubt due to pneumatic effects associated with interstitial air.

Takahasi (1937) studied the gravity flow of various dry sands in a straight chute of rectangular cross-section at various angles of inclination. He noticed two flow regimes: one which consisted of an upper thin layer of particles flowing over a stationary layer overlying the chute bed and a second where all the particles were in motion, each particle following a chaotic fluctuating path and interacting vigorously with its neighbours. The velocity of particles (estimated from their trajectories) leaving the downstream end of the channel increased rapidly with inclination angle for the first flow regime and much less rapidly for the second. Takahasi drew attention to the similarities between these experiments and natural phenomena such as snow avalanches and land slides (see Scheidegger 1975, chaps. 4 and 5 for a recent discussion of such catastrophic events).

Roberts (1969) studied the flow of millet seed in Perspex chutes of rectangular

cross-section. By using high-speed ciné photography (1200–2000 frames/s), he found that, although the grains slipped on the smooth Perspex chute walls, a small velocity gradient existed over the depth of the granular flow. Roberts assumed that the granular flow was analogous to the sliding of a block on a rough incline. Using an effective angle of friction between the grains and the channel (which accounts for friction on the side walls as well as the bottom) and assuming the bulk to be incompressible, Roberts developed a simple analysis which gives the variation of the depth-averaged velocity and the flow thickness with downstream distance. The effective friction angle was measured under quasi-static conditions and assumed to be velocity independent. For a straight inclined chute Roberts' analysis predicts that the flow accelerates, decelerates or remains uniform when the effective friction angle is respectively less than, greater than or equal to the chute angle of inclination.

Ridgway & Rupp (1970) examined the flow of various sands down a brass chute of rectangular cross-section. Particles of three different size ranges (250–355 μm, 420–500 μm and 758–850 μm) were obtained by sieving. Most of the experiments shown were for very shallow depths of granular flow of 2–3 mm (corresponding to only a few particle 'diameters'). For chute inclination angles between 30 and 60° the flow accelerated down the 1 m length of chute. Particle velocities were determined with a high speed ciné camera by filming from above the free surface and from below through a glass section in the bed of the chute. No velocity gradient over the depth was evident. Ridgway & Rupp attempted to determine bulk density profiles by positioning a horizontal knife-edge at different depths and weighing the flows collected in a given time from above and below the knife-edge. With the assumption of a uniform velocity profile, the density profile was then calculated. It was found that the density decreased with distance downstream, more so for the larger particles than for the smaller ones. Ridgway & Rupp also determined that the density varied considerably over the depth, typically from a low value of about 0·2 g/c.c. (about 15 % of the stationary poured bulk density) at the bed to a maximum roughly at the mid-depth of about 1·0 g/c.c. (about 65 % of the stationary poured bulk density). Because of considerable particle saltation the bulk density dropped gradually to zero near the free surface, where a 'surface cloud' of particles was observed. Owing to the large size of the particles relative to the depth (thus relative to the gap between the bed and the knife-edge) and the likelihood of an upstream effect of the knife-edge flow divider, the density profiles presented by Ridgway & Rupp may be unreliable.

Suzuki & Tanaka (1970) endeavoured to use the inclined chute as a viscometer for particulate materials. To do this requires *a priori* an assumption as to the form of the constitutive equation. Suzuki & Tanaka assumed that the bulk solid behaved as a Bingham fluid with a constant yield stress and a constant viscosity. This is unrealistic since, first, the bulk solids behave as a Coulomb material in which the yielding is influenced by the hydrostatic pressure [see (1.1)], and second, the experiments of Bagnold (1954) indicate that the stresses are related to the strain rates in a nonlinear way.

Augenstein & Hogg (1974) determined the friction angles between thin layers of sand particles and both a smooth and a sand-roughened inclined steel chute by using the velocity variation along the chute in conjunction with a simple analysis similar to that given by Roberts (1969). The velocities were estimated from the trajectories of particles leaving the end of the chute.

1.3. *Previous work related to constitutive equations for rapidly flowing granular materials*

Over 20 years ago Bagnold (1954) performed experiments on neutrally buoyant spherical particles suspended in Newtonian fluids (water and a glycerine–water–alcohol mixture) and sheared in a coaxial rotating cylinder apparatus. Both the torque and the normal stress in the radial direction were measured when various concentrations of the spherical grains were sheared. Bagnold distinguished two limiting types of behaviour. In the so-called *macro-viscous* region (corresponding to low shear rates), which is dominated by fluid viscosity, the shear and the normal stress are linear functions of the velocity gradient. Of primary present concern is the *grain-inertia* region, in which the fluid in the interstices plays a minor role and the dominant effects arise from particle–particle interactions. Both the shear and the normal stresses in this region are proportional to the square of the velocity gradient. The interesting phenomenon was the presence of a normal stress (which Bagnold termed the dispersive pressure) proportional to the shear stress, reminiscent of the quasi-static behaviour of a cohesionless Coulomb material [equation (1.1)]. For the *grain-inertia* region Bagnold presented a simple analysis, roughly analogous to kinetic gas theory, to predict the normal (dispersive) pressure and the shear stress. He neglected the suspending fluid phase and considered the interaction of two layers of spherical grains of diameter D in a shear flow $U(y)$ as shown in figure 1. The mean distance between centres is bD and the resulting free distance is s. Then

$$b = 1 + s/D = 1 + 1/\lambda, \tag{1.2}$$

where λ is the 'linear concentration'. The volume concentration may be expressed as

$$C = \frac{C_0}{b^3} = \frac{C_0}{(1+1/\lambda)^3}, \tag{1.3}$$

where C_0 is the maximum possible concentration when $\lambda = \infty$ (for spheres

$$C_0 = \pi/3\sqrt{2} = 0{\cdot}74).$$

Bagnold's analysis indicated that the normal stress in the y direction was

$$P = a\rho_s \lambda f(\lambda)\, D^2 (dU/dy)^2 \cos\alpha_i \tag{1.4}$$

and the grain shear stress was

$$S = P\tan\alpha_i, \tag{1.5}$$

where ρ_s is the grain density, f is an unknown function of λ, a is a constant and α_i is an unknown angle dependent upon collision conditions. (Similar results follow directly from dimensional analysis.) At the higher shear rates (in the *grain-inertia* region) the experimental shear stress varied with dU/dy as predicted by (1.4) and (1.5) and Bagnold was able to determine a, α_i and $f(\lambda)$. For $\lambda < 14, f = \lambda$, and for $\lambda > 14, f$ increases very rapidly with λ. Large λ corresponds to the grains being close together; if λ is large enough the grains lock together and very large stresses are required to shear the bulk. The angle α_i was found to vary only slightly with λ.

Bagnold applied these results to predict the flow of dry sand down an incline, the bulldozing of a mass of sand and the 'singing' mechanism in desert dunes (Bagnold 1954, 1966). Despite its fundamental importance, Bagnold's work seems to have gone unnoticed by workers concerned with flow of bulk solids until recently.

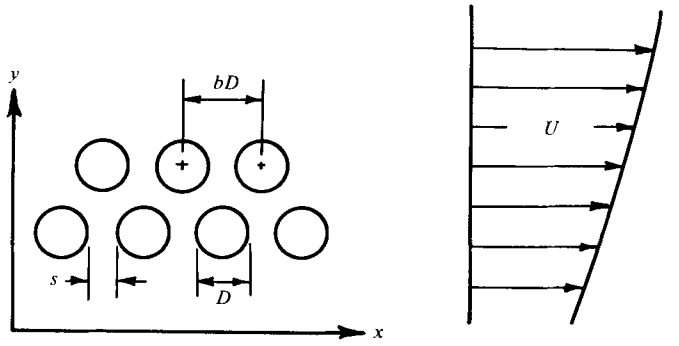

FIGURE 1. Definition sketch for Bagnold's (1954) theory of stresses in the *grain-inertia* region.

Bridgwater (1972) developed an annular dynamic shear cell to measure the effects of the rate of strain upon stresses in various particulate solids. With the axis of rotation vertical, loading weights maintained a constant (vertical) normal stress and torques were measured at various rates of rotation of the lower half of the annular shear cell. Although the results, as presented, initially suggest only a small 'velocity dependence' of the stresses, further consideration reveals that they confirm in part Bagnold's (1954) results. In the *grain-inertia* region Bagnold found that both the dispersive normal stress and the shear stress increased with λ and dU/dy but that $\tan\alpha_i$, the ratio of the shear stress to the normal stress, remained almost constant. In Bridgwater's apparatus the normal stress was fixed and since the bulk solid could expand vertically (decreasing λ) little variation of the shear stress with the shear rate is to be expected.

Goodman & Cowin (1971, 1972) have developed a continuum theory for the representation of the stresses developed during the flow of granular materials. The theory is intended for situations where the stress levels are less than 10 psi (Cowin 1974*a*) and where pneumatic effects are negligible. The non-dissipative part of the stress tensor is related to the fractional solids content ν and the gradients of ν. The dissipative part is assumed to behave as a Newtonian fluid. On the basis of Bagnold's work (1954, 1966) this last assumption is doubtful, but as Cowin (1974*a*) points out, the theory can be extended without affecting the non-dissipative part of the stress tensor. The theory has been 'linearized' and specialized to the case of incompressible granules (Goodman & Cowin 1971, 1972) and it was shown that for limiting equilibrium the resulting constitutive equation describes a Mohr–Coulomb material (see also Cowin 1974*b*). The theory for cohesionless materials with incompressible grains has been applied to the problems of granular flow down an inclined plane and between vertical parallel plates (Goodman & Cowin 1971). Apart from the assumption of Newtonian behaviour for the dissipative part of the stress tensor, the solutions to these problems were based upon a special case of the linear theory which contains certain inconsistencies. These inconsistencies have been rectified in a later paper by Cowin (1974*a*).

Because of the Newtonian flow assumptions, Goodman & Cowin (1971) found that steady, fully developed, uniform depth, open-channel flows were possible for all channel inclinations greater than the angle of repose of the material. Their theory

also required a plug flow in the central region of flow between parallel plates in order to satisfy the steady equations of motion.

As a final complication, there is the question of whether or not smooth steady velocity profiles exist during granular flow at low stress levels. Recently Lee *et al.* (1974) have suggested that two flow regimes exist: one comprised of essentially incompressible rigid-body motions and the other consisting of narrow shear zones which partition regions of the first type.

The foregoing discussion has attempted to indicate the unsettled state of the mechanics of flow of granular materials, particularly for cases when the material is undergoing rapid deformations such that inertia and strain-rate effects are important. The present paper describes both theoretical and experimental studies which endeavoured to clarify certain aspects of granular flow. While the main orientation of the paper is towards the development of realistic constitutive equations, the work described is also of intrinsic practical importance with regard to bulk solids transport. The paper begins with an account of some preliminary exploratory experiments on granular flow down a long inclined chute. A constitutive equation is proposed and used for the analysis of two simple two-dimensional shear flows: free-surface flow down an inclined chute and flow down a vertical channel. An attempt to produce these two flows experimentally was made and velocity profiles for various flow conditions are presented. Finally, granular jumps, which are analogous to open-channel hydraulic jumps, are discussed.

2. Preliminary experiments

Some exploratory experiments were performed and it is worth recording the results of these tests as a preliminary to the detailed theoretical and experimental studies described in later sections. In these preliminary experiments surface velocity profiles and depth profiles were measured during free-surface flow down an inclined channel.

A diagramatic sketch of the apparatus is shown in figure 2. The flow channels were made from a 6·1 m length of a 5×5 in. (nominal) aluminium I-beam turned on its side. The surface of one of the channels formed by the I-beam was left smooth while the channel on the reverse side of the I-beam was roughened by glueing sand grains (about 0·5 mm mean diameter) to its surface. The upper end of the I-beam rested on a pivot support so that the angle of inclination ζ could be varied. The bulk solid was Ballotini spherical glass beads with a diameter of 0·42–0·59 mm and a specific gravity of 2·90. The beads entered the flow channel smoothly from a transition section attached to the bottom hopper portion of the supply bin. The flow rate was regulated by the insertion of calibrated orifice plates in the lower end of the hopper.

2.1. *Surface velocity profiles*

The velocity profiles across the width of the channel at the free surface were indicated by thin lines of coloured beads dropped periodically onto the free surface by a bead injector which could be installed at various stations directly above the channel. The velocity profiles were also determined by filming the flow with a Bolex 16 mm ciné camera (typically at 64 frames/s). The granular material for these tests consisted of a small percentage of coloured beads mixed with uncoloured ones. By measuring the

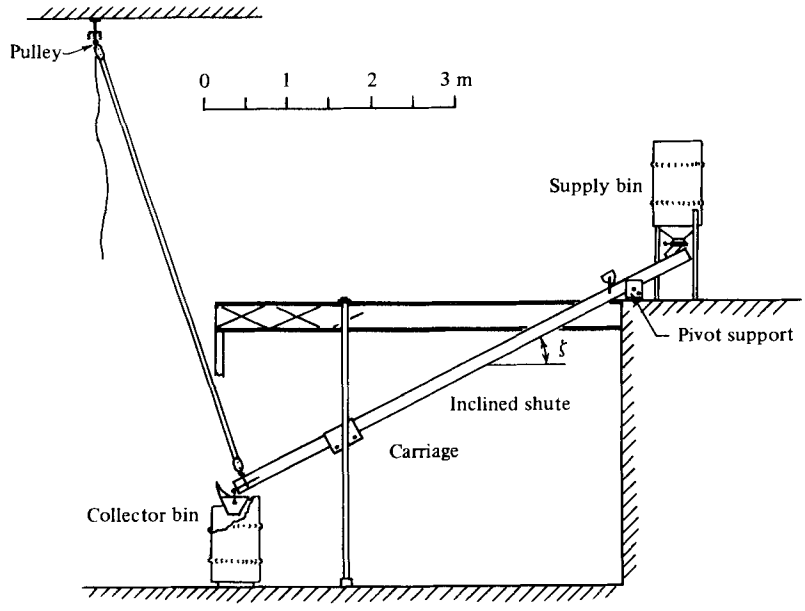

FIGURE 2. Schematic diagram of inclined-chute apparatus used for preliminary exploratory experiments.

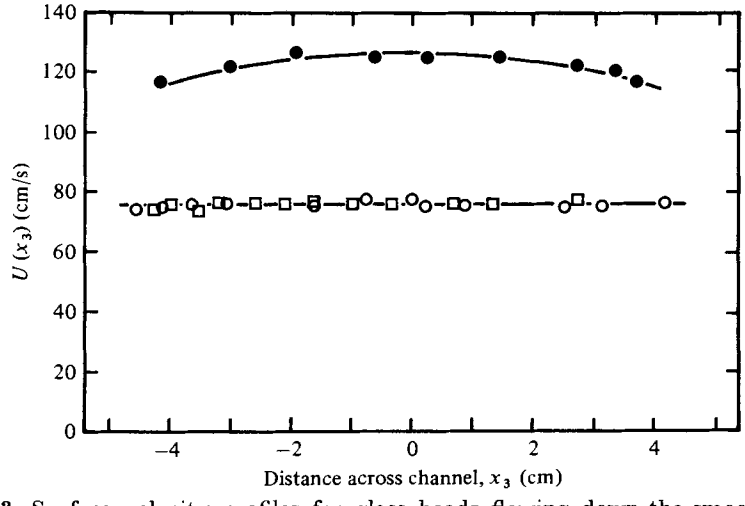

FIGURE 3. Surface velocity profiles for glass beads flowing down the smooth-walled 10·8 cm wide inclined chute. Measurements made at station 2·97 m from entry at a mass flow rate of 0·89 kg/s. ○, □, runs 1 and 2 respectively for $\zeta = 18{\cdot}8°$, $h = 1$ cm; ●, $\zeta = 20{\cdot}2°$, $h = 0{\cdot}65$ cm.

distance that individual particles travelled between successive frames of the film, the velocity profiles were ascertained.

For the smooth-walled channel, considerable slip occurred at the walls. The wall friction angle ($\sim 18°$) was less than the internal friction angle ($\sim 23°$) for the glass beads and plug flow with a virtually uniform velocity resulted. The case $\zeta = 18{\cdot}8°$ in figure 3 is typical of the profiles at lower channel inclinations and larger depths.

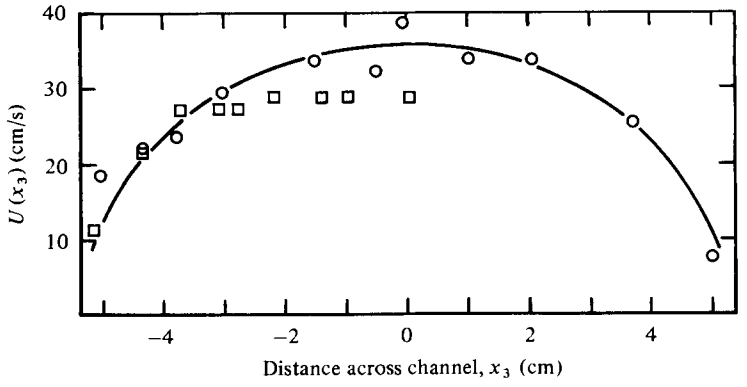

FIGURE 4. Surface velocity profile for glass beads flowing down the rough-walled 10·8 cm wide inclined chute. Measurements made at station 2·97 m from entry at a mass flow rate of 0·56 kg/s. ○, □, runs 1 and 2 respectively for $\zeta = 23{\cdot}3°$, $h = 2{\cdot}2$ cm.

With an increase in slope and/or decrease in the depth h, slip still occurred at the walls but a slight shear developed in the interior of the flow (see, for example, the case $\zeta = 20{\cdot}2°$ in figure 3). For small depths and steep inclinations the bulk density appeared to be quite low and particles moved in a saltation mode, with a 'cloud' of particles near the 'surface' similar to that described by Ridgway & Rupp (1970).

For the rough-walled channel it appeared that something close to a no-slip condition was produced at the walls and a blunt velocity profile developed in a short distance from the channel entrance. Individual particles near the free surface followed random fluctuating paths. The frame analysis of the ciné film was extremely tedious since it proved necessary to average a large number of frames in order to obtain definitive mean velocity profiles.

A typical rough-wall velocity profile is shown in figure 4. Each data point shown results from an average of four frames taken with the ciné camera running at 64 frames/s. Because of the short averaging time considerable 'scatter' is present, but the general shape of the mean velocity profile and a rough idea of the magnitude of the velocity fluctuations are evident.

It was found that lines of coloured beads placed on the surface by the bead injector deformed with downstream distance in the manner shown schematically in figure 5(*a*). The originally straight time lines, which developed initially into quite smooth but blunt profiles, became sharper and more peaked with increasing time. Such behaviour indicated the presence of slow secondary flows moving at the surface from the side walls towards the channel centre-line (figure 5*b*), since the surface streamwise velocity profiles were found to be similar at various downstream stations. When small patches of coloured beads were placed on the surface near the side wall they were found to move slowly towards the centre-line while travelling downstream, giving further evidence of the secondary flows.

2.2. *Depth profiles*

The variation of flow depth with downstream distance was measured for several flow rates in both the smooth- and the rough-walled channel by means of a movable depth gauge mounted on the top of the flow channel.

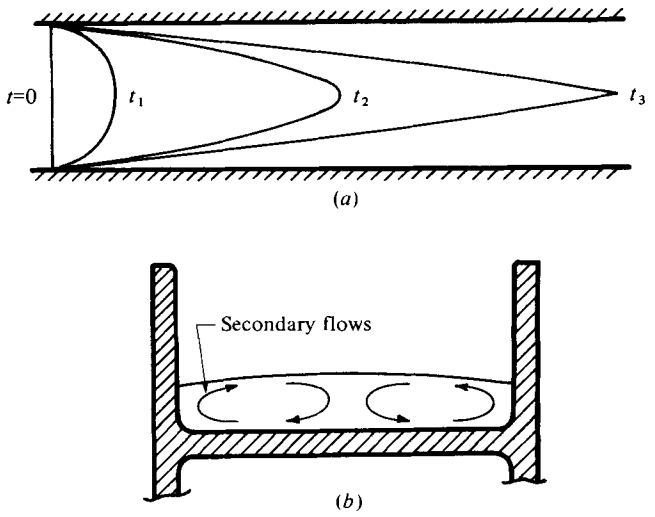

FIGURE 5. (*a*) Schematic diagram of time lines at free surface during flow in rough-walled inclined chute. (*b*) Inferred secondary flow patterns.

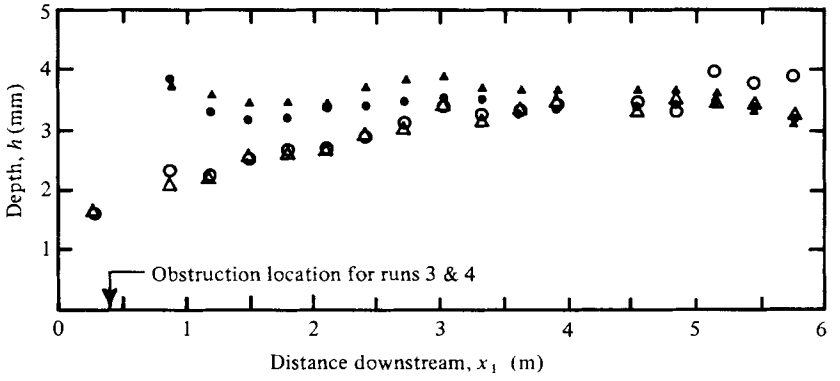

FIGURE 6. Depth profiles for glass beads flowing down the smooth-walled 10·8 cm wide inclined chute at a mass flow rate of 0·56 kg/s and $\zeta = 20{\cdot}1°$. ○, △, runs 1 and 2 respectively for channel free of obstructions; ●, ▲, runs 3 and 4 respectively with obstruction placed on chute bed 0·4 m from entry.

Some depth profiles for smooth walls are shown in figure 6. Results for two test conditions are plotted; in one case the channel was unobstructed and in the other a wedge-sectioned strip with a vertical upstream face 0·5 cm high was placed on the channel bottom across the flow, 0·4 m from the channel entrance. For the unobstructed case, the flow decelerates after entering the channel and the depth gradually increases and approaches a uniform value at a downstream distance of about 4 m. The purpose of the obstruction was to cause an increase in the flow depth close to the channel entrance. Despite the larger 'initial' depth the flow was found to approach the same uniform depth as for the smooth unobstructed channel. The fact that the same uniform depth was approached from both above and below implies the existence of a 'normal depth' in the sense that the term is used in hydraulics. This result is in contradiction with the theory of Roberts (1969), in which the acceleration of the depth-averaged

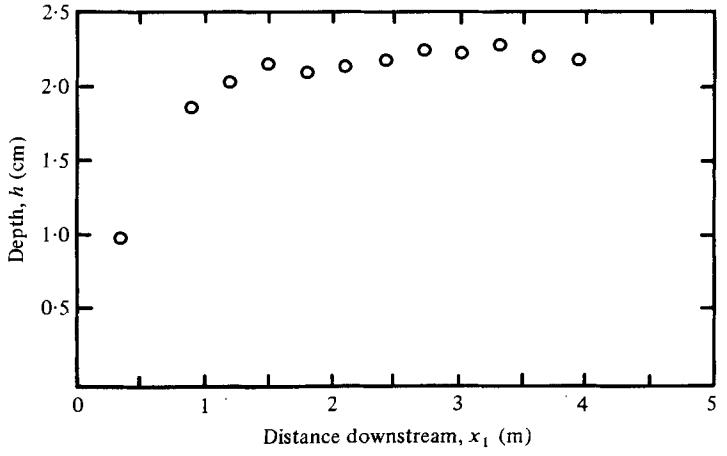

FIGURE 7. Depth profile for glass beads flowing down the rough-walled 10·8 cm wide inclined chute at a mass flow rate of 0·56 kg/s and $\zeta = 23{\cdot}6°$.

flow is constant. However, it should be noted that in tests performed at flow rates a few times larger than that of figure 6, resulting in higher initial depths, the mean flow did accelerate and flow depths decreased with streamwise distance.

In the unobstructed smooth-wall tests the flows were 'supercritical' (Froude number > 1). Surge waves and 'granular jumps' analogous to hydraulic jumps could be formed by placing obstructions or controls at the downstream end of the channel. Even in the absence of any obstructions, occasionally surge waves were spontaneously generated at the downstream end of the channel. They moved upstream for distances of up to 1·5 m and were then swept back downstream again. The mechanism responsible for the generation of these spontaneous surge waves is unknown. A detailed discussion of the granular jumps is presented later in § 7.

Figure 7 shows a typical depth profile for rough walls. The flow decelerates after entry and reaches the 'normal depth' in a relatively short distance.

A short 16 mm ciné film showing the velocity profiles, surge waves, granular jumps and other phenomena is available on loan from the author.

Some of the more salient aspects of the flows disclosed by these preliminary experiments may be summarized as follows:

(*a*) Although considerable slip of the granular material occurs at smooth walls, the no-slip condition may be approached by applying wall roughness of the same order as the particles making up the bulk solid.

(*b*) Relatively smooth velocity profiles occur during flow down an inclined chute The flow is unlike the slow initial flow in hoppers observed by Lee *et al.* (1974), which consisted of the movement of irregular rigid regions partitioned by narrow shear zones.

(*c*) 'Normal' depths appear to exist for free-surface flows. This implies a shear-rate dependence in the constitutive equation.

(*d*) Secondary flows develop during flow down the chute. They are reminiscent of those predicted by Green & Rivlin (1956) for certain non-Newtonian fluids which exhibit 'normal-stress effects'.

3. Constitutive equations

The continuum theory described in this section is intended to represent the flow of granular materials at relatively low stress levels and high shear rates such that the bulk behaviour is governed by interparticle friction, collisions and other interactions corresponding to the *grain-inertia* regime of Bagnold (1954). The theory is *not* intended to represent the stresses when the rate of deformation becomes zero (the 'equilibrium' state of Goodman & Cowin 1972). The effects of the fluid contained in the interstices and electrostatic adhesion are assumed to be negligible (this implies that the bulk solid consists of relatively large particles of fairly uniform size). It is proposed that an appropriate theory should (*a*) reflect the Mohr–Coulomb behaviour, where the shear stress is proportional to the normal stress, and (*b*) relate the stresses to the strain rates in a non-Newtonian way in accordance with the experiments of Bagnold (1954).

A preliminary version of the present theory was delivered at Euromech Colloquium 84 on *Mechanics of Granular Materials*, Warsaw, Poland in 1976. Professor Stephen Cowin (Department of Mechanical Engineering, Tulane University, New Orleans) subsequently advised me that this formulation was incomplete since certain terms in the constitutive equation had been omitted. We have collaborated in writing the following subsection in an attempt to present the theory in a form which is more complete as well as more direct.

3.1. *A nonlinear theory for flowing granular materials*

By Stephen C. Cowin and Stuart B. Savage

A simple and general theory for flowing granular materials with relatively rigid grains is presented here. This theory has some similarity to the theory presented by Goodman & Cowin (1971, 1972), but the presently proposed theory is more general because it makes fewer, less restrictive assumptions. Goodman & Cowin proposed that one density field $\rho(\mathbf{x}, t)$ be interpreted as a bulk density which can be expressed as the product of the fields ν and γ,

$$\rho = \nu\gamma, \tag{3.1}$$

where $\gamma(\mathbf{x}, t)$ is the actual density of the grains at the place $\mathbf{x}$ at time t and $\nu(\mathbf{x}, t)$ is the volume fraction of solids at the place $\mathbf{x}$ at time t. The field $\nu(\mathbf{x}, t)$ is called the volume distribution and it is related to the porosity n or the void ratio e by

$$\nu = 1 - n = (1 + e)^{-1};$$

of course $0 < \nu < 1$. The representation (3.1) for the density introduces an additional kinematic variable into the structure of the classical continuum theories. In the classical continuum theories the density ρ is determined from the continuity equation

$$\dot{\rho} + \rho \operatorname{div} \mathbf{v} = 0, \tag{3.2}$$

and the velocity $\mathbf{v}(\mathbf{x}, t) = u_i(x_i, t)\,\mathbf{e}_i$ is determined from the conservation of linear momentum

$$\rho\dot{\mathbf{v}} = \operatorname{div} \mathbf{T} + \rho\mathbf{b} \tag{3.3}$$

using a constitutive equation relating the stress to the gradients of the velocity or displacement fields. The term $\mathbf{b}$ in (3.3) represents the body force. Equations (3.2) and (3.3) can be viewed as a system of four scalar equations in four scalar unknowns,

the density and the three velocity components. The introduction of the compound representation (3.1) of the density introduces another unknown in the theoretical structure. As a consequence of a variational study that was subsequently published (Cowin & Goodman 1976), Goodman & Cowin (1971, 1972) proposed an additional equation. However, it has been recently pointed out to the writers by Professor J. T. Jenkins (Department of Theoretical and Applied Mechanics, Cornell University) that when the additional assumptions of (*a*) a cohesionless material with (*b*) incompressible grains and (*c*) a free energy function linear in $|\text{grad}\,\nu|^2$ are made, the theory of Goodman & Cowin (1971, 1972) is so constrained that few solutions of interest are obtained. As we wish to consider here the flow of a cohesionless material with incompressible grains, we shall formulate a theory similar to that of Goodman & Cowin (1971, 1972), but one which makes fewer and less restrictive assumptions. The present development will avoid the extra equation of Goodman and Cowin by using the assumption of grain incompressibility to reduce the number of independent field variables to four.

The assumption of grain incompressibility is written

$$\gamma = \text{constant}. \tag{3.4}$$

It follows from (3.2), using (3.1) and (3.4) that

$$\dot{\nu} + \nu \,\text{div}\,\mathbf{v} = 0 \tag{3.5}$$

Thus, rather than seeking an additional equation to govern the additional variable as Goodman & Cowin did, the constant grain density γ is eliminated as an independent field variable and there are then four scalar equations, (3.3) and (3.5), to determine four scalar unknowns, $\mathbf{v}$ and ν, assuming the existence of a constitutive relation for $\mathbf{T}$ which completely determines $\mathbf{T}$ as a function of $\mathbf{v}$ and ν and their derivatives. Thus, to complete the system of governing equations we assume that the stress is an isotropic function of ν_0, ν, grad ν and the rate of deformation $\mathbf{D}$,

$$\mathbf{T} = \mathbf{T}(\nu_0, \nu, \text{grad}\,\nu, \mathbf{D}) \tag{3.6}$$

where $\mathbf{D}$ is given by

$$2\mathbf{D} = \text{grad} \otimes \mathbf{v} + \mathbf{v} \otimes \text{grad} \tag{3.7}$$

and where ν_0 is a reference value of the volume fraction ν. Given that γ and the body force $\mathbf{b}$ are known, the system of equations (3.3), (3.5) and (3.6) is a system of ten scalar equations for the ten scalar unknowns ν, $\mathbf{v}$ and $\mathbf{T}$.

The form of the dependence of the stress $\mathbf{T}$ upon grad ν and $\mathbf{D}$ can be made more explicit using the assumed isotropic dependence of $\mathbf{T}$ upon grad ν and $\mathbf{D}$. To do this we introduce the notation

$$\mathbf{M} = (\text{grad}\,\nu) \otimes (\text{grad}\,\nu) \tag{3.8}$$

and observe that

$$tr\,\mathbf{M} = |\text{grad}\,\nu|^2, \quad \mathbf{M}^2 = (tr\,\mathbf{M})\,\mathbf{M} = |\text{grad}\,\nu|^2\,\mathbf{M}. \tag{3.9}$$

The constitutive relation (3.6) may be written

$$\mathbf{T} = a_0\,\mathbf{I} + a_1\,\mathbf{D} + a_2\,\mathbf{M} + a_3(\mathbf{MD} + \mathbf{DM}) + a_4\,\mathbf{D}^2 + a_5(\mathbf{MD}^2 + \mathbf{D}^2\,\mathbf{M}) \tag{3.10}$$

where a_0–a_5 are functions of ν_0, ν, $tr\,\mathbf{M}$, $tr\,\mathbf{D}$, $tr\,\mathbf{D}^2$, $tr\,\mathbf{MD}$ and $tr\,\mathbf{MD}^2$. This representation for $\mathbf{T}$ follows from the formula for the reduction of a matrix polynomial of two matrices (cf., for example, Green & Adkins 1960, pp. 315–318). The complicated form of $\mathbf{T}$ given by (3.10) may be necessary if it is found that certain kinds of normal stress

effects (Truesdell 1974) are displayed by flowing granular materials. At this time there are insufficient experimental data available to settle the question. For the present paper we make use of a simpler form in which $\mathbf{T}$ depends linearly on the strain rate tensor $\mathbf{D}$. It will be shown that this is sufficient to model the main features of material behaviour in the grain inertia regime that have been reported by Bagnold (1954, 1966). In this case (3.10) reduces to

$$\mathbf{T} = a_0\,\mathbf{I} + a_1\,\mathbf{D} + a_2\,\mathbf{M} + a_3(\mathbf{M}.\mathbf{D} + \mathbf{D}.\mathbf{M}). \tag{3.11}$$

Equation (3.11) is still extremely general and further assumptions regarding the explicit functional dependence of a_0, a_1, a_2 and a_3 upon ν_0, ν, $tr\,\mathbf{M}$, $tr\,\mathbf{D}$ and $tr\,\mathbf{MD}$ are required before it can be used for the prediction of various flow situations. Physical discussions providing some justification for these assumptions are presented in the following subsections.

3.2. *The 'equilibrium stress'*

By Stuart B. Savage and Stephen C. Cowin

In this subsection we present some heuristic arguments to restrict the coefficients a_0 and a_2 appearing in (3.11). We shall consider the problem of associating the stress state obtained from (3.11) as $\mathbf{D} \to 0$ with limiting equilibrium in granular materials. Cowin (1974*b*) showed that constitutive equations which were isotropic functions of $\mathbf{D}$ and a single vector argument satisfied a generalized Mohr–Coulomb type yield criterion as $\mathbf{D} \to 0$. The proof of Cowin applies to the constitutive equation (3.11). We shall require that (3.11) satisfies a traditional Mohr–Coulomb condition as $\mathbf{D} \to 0$ and this will permit us to associate part of a_0 and a_2 with the angle of internal friction ϕ and the cohesion c introduced in (1.1). The requirement that the traditional Mohr–Coulomb condition be satisfied by $\mathbf{T}$ as given by (3.11) in the limit as $\mathbf{D} \to 0$ yields the following representations for a_0 and a_2

$$a_0 = c\cot\phi - p + a_0' \quad \text{and} \quad a_2 = -2\alpha + a_2', \tag{3.12}$$

where

$$p = \alpha\left(\frac{1}{\sin\phi} - 1\right) tr\,\mathbf{M} \tag{3.13}$$

and where α, c and ϕ depend upon ν_0, ν and $tr\,\mathbf{D}$ but not upon $tr\,\mathbf{M}$ or $tr\,\mathbf{MD}$; and a_0' and a_2' depend upon ν_0, ν, $tr\,\mathbf{D}$, $tr\,\mathbf{MD}$, but they must vanish as $\mathbf{D} \to 0$. The following representation for the stress

$$\mathbf{T} - \mathbf{T}_0 = a_0'\,\mathbf{I} + a_1\,\mathbf{D} + a_2'\,\mathbf{M} + a_3(\mathbf{M}.\mathbf{D} + \mathbf{D}.\mathbf{M}), \tag{3.14}$$

where

$$\mathbf{T}_0 = (c\cot\phi - p)\,\mathbf{I} - 2\alpha\,\mathbf{M}, \tag{3.15}$$

is obtained from (3.11) when (3.12) is employed. We might regard $\mathbf{T}_0$ as an 'equilibrium stress' in the sense that it is equal to $\mathbf{T}$ as $\mathbf{D} \to 0$.

We shall now show that the stress $\mathbf{T}_0$ specified by (3.15) satisfies the Coulomb failure criterion. The stress vector $\mathbf{t}$ acting on a surface whose normal is $\mathbf{n}$ is given by (3.15) as

$$\mathbf{t} = \mathbf{T}_0\,\mathbf{n} = (c\cot\phi - p)\,\mathbf{n} - 2\alpha\frac{\partial\nu}{\partial n}\operatorname{grad}\nu. \tag{3.16}$$

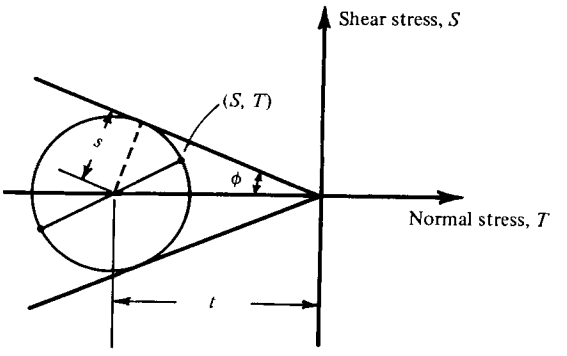

FIGURE 8. Mohr's circle representation of equilibrium stresses T^0_{ij}.

The normal stress component on the plane whose normal is $\mathbf{n}$ is $\mathbf{t}.\mathbf{n}$, thus we define T by

$$T = \mathbf{t}.\mathbf{n} = c\cot\phi - p - 2\alpha\left(\frac{\partial\nu}{\partial n}\right)^2. \tag{3.17}$$

The square of the magnitude of $\mathbf{t}$, $\mathbf{t}.\mathbf{t}$, is equal to the sum of the square of the normal stress T acting on $\mathbf{n}$ and the square of the shear stress S acting on the plane whose normal is $\mathbf{n}$, thus from (3.16)

$$T^2 + S^2 = \mathbf{t}.\mathbf{t} = (c\cot\phi - p)^2 - 4\alpha(c\cot\phi - p)\left(\frac{\partial\nu}{\partial n}\right)^2 + 4\alpha^2\left(\frac{\partial\nu}{\partial n}\right)^2 |\operatorname{grad}\nu|^2. \tag{3.18}$$

This representation can be rewritten in the form

$$S^2 + (T-t)^2 = s^2 \tag{3.19}$$

where

$$s = \alpha tr\,\mathbf{M} = \alpha|\operatorname{grad}\nu|^2; \tag{3.20}$$

$$t = c\cot\phi - p - \alpha tr\,\mathbf{M} = c\cot\phi - p - \alpha|\operatorname{grad}\nu|^2. \tag{3.21}$$

The result (3.19) shows that the stress state $\mathbf{T}^0$ has a Mohr's circle representation with radius s located at $(t, 0)$ in the (T, S) plane. Elimination of $\alpha|\operatorname{grad}\nu|^2$ between (3.20) and (3.21) yields a traditional representation of the Coulomb yield condition

$$s = \sin\phi(c\cot\phi - t). \tag{3.22}$$

This expression can be converted to a representation in terms of S and T on the failure surface by use of the formulas

$$s = |S|/\cos\phi, \quad t = T - |S|\tan\phi \tag{3.23}$$

which hold there at limiting equilibrium.
Thus (3.22) may be reduced to

$$|S| = c - T\tan\phi. \tag{3.24}$$

[Note that here we use the sign convention that tensile stresses are positive. This is opposite to the usual soil mechanics and is responsible for the difference in sign arising between (3.24) and (1.1).]

In the remainder of this work we assume that the material is cohesionless and thus that c is zero. The representation of (t, s) and (T, S) in the Mohr's circle plane is shown in figure 8.

Although the Mohr–Coulomb type behaviour expressed by (3.19)–(3.24) is an attractive feature of the theory, there is another aspect that is less plausible if $\mathbf{T}_0$ is to be regarded as the stress developed at limit equilibrium (in the sense that the term is used in soil mechanics). Taking the cohesion c to be zero in (3.15) we note that if

$$(\mathbf{T}_0)_{ij} = T^0_{ij} = -p\,\delta_{ij} - 2\alpha\nu_{,i}\nu_{,j}$$

is to be non-zero for $i \neq j$, then both $\nu_{,i}$ and $\nu_{,j}$ must be non-zero.

The resulting dilemma is illustrated by the following example. Consider the situation of a Rankine stress state (Terzaghi 1963, pp. 29–32) associated with a granular material which is in a state of limit equilibrium and has an inclined plane free surface of large extent. The equations of static equilibrium require the existence of a shear stress everywhere below the free surface in a direction parallel to the free surface and in the plane formed by the body-force vector and the normal to the free surface. It may be reasonable on physical grounds to expect no variations of ν in directions parallel to the free surface. If this is so then (3.15) is incapable of yielding the shear stress required for static equilibrium.

Nevertheless this may not be a major concern if we are interested only in flow situations. We consider the state at limit equilibrium to be essentially different from that where flow occurs, however slowly. For example, in the preliminary tests with the rough-walled channel (§ 2) inclined at angles slightly less than the angle or repose, material of uniform depth would remain motionless in the channel in the absence of an external disturbance. However, by manually giving the material a push it could be made to flow slowly but continuously and uniformly at constant depth. Thus two different flow states existed at the same channel inclination (but presumably at different values of ν).† In both cases the inertia forces were zero and equilibrium was established by a balance between the shear stresses and the body-force components in the streamwise direction. The shear stresses result from different mechanisms; in the static case they result from dry interparticle friction and particle interlocking whereas in the shear-flow case particles override other particles and the inertia associated with interparticle collisions becomes more important. In other words the static and flowing cases may be regarded as two different states, rather like (metaphorically speaking) a solid and a liquid when viewed on the microscopic scale. There is not a smooth transition from one state to another as $\mathbf{D} \to 0$ and thus a constitutive equation suitable for flowing materials need not necessarily be appropriate to describe the state of static equilibrium. With this in mind we interpret the stress $\mathbf{T}_0$ given by (3.15) merely as an additional component of stress arising during the deformation of the bulk solid because of a non-uniform ν. It may formally be obtained from $\mathbf{T}$ by setting $\mathbf{D}$ to zero (a more careful definition will be given subsequently).

The theory of § 3.1 was derived by first postulating that the response of the granular material depends upon grad ν (among other things) and then proceeding with the formal arguments of continuum mechanics. Although there is evidence to suggest some relationship between ν and the stresses (see for example the discussion by Cowin 1974*a*) it is not physically obvious nor has it been suggested previously (in terms of specific mechanical or physical models) why the stresses should depend upon the gradients of ν. By considering individual particle interactions a rather crude physical argument for the presence of such a dependence may be postulated. The following

† A related phenomenon of avalanching on sand dunes has been discussed by Allen (1970).

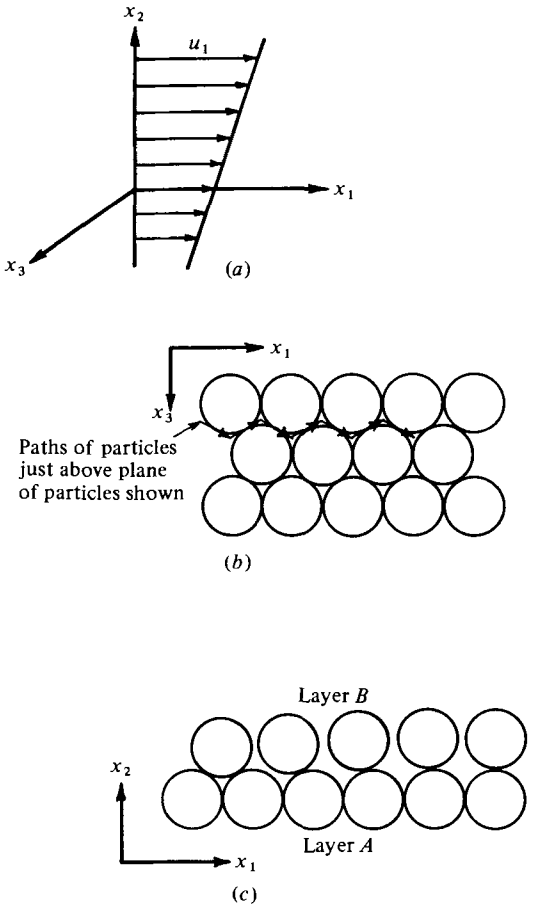

FIGURE 9. Simple interpretation of ν-gradient stresses. (*a*) Shear flow $u_1(x_2)$. (*b*) Plan view of regularly packed particles of layer A in x_1, x_3 plane. (*c*) Elevation view (x_1, x_2 plane) of 'shearing' motion when $\partial\nu/\partial x_2 \neq 0$. Because of the gradient of ν in the x_2 direction, layers of particles cannot readily pass over each other; local dilations and increased stresses result.

discussion provides a reinterpretation of the 'equilibrium' stress of Goodman & Cowin as well as some physical justification for the detailed functional form to be assumed for (3.14).

Consider a shear flow $u_1(x_2)$ as shown in figure 9 (*a*) between plane layers of regularly packed particles of equal diameter. For very close packing and uniform ν, in the layer (layer B) just above layer A the individual particles follow the zigzag paths indicated in figure 9 (*b*). The spacings in both layers are the same and particles in layer B can move through the 'valleys' between particles in layer A.

For the case where there are gradients of ν (the case of non-zero $\partial\nu/\partial x_2$ is shown), the spacing of particles in layers A and B are different and there occur regions as shown in figure 9 (*c*) where local dilations and normal stresses are generated when the two layers are sheared. Because of the 'frictional' nature of the bulk solid, normal 'stresses' in the x_1 and x_3 as well as the x_2 direction are generated. According to (3.13), (3.15) and (3.19)–(3.22) their magnitudes depend upon the internal friction angle ϕ. The situation shown at the right-hand side of figure 9 (*c*) is analogous to a 'centre of

dilation'. It is pertinent to take note of a model of a centre of dilation for the continuum theory of dislocations discussed by Eshelby (1951) in which an elastic sphere is forced into a spherical hole of slightly smaller diameter in an infinite elastic medium.

The above argument is somewhat simplistic and should be regarded as suggestive rather than precise. In the real case the particles will not be regularly spaced and interparticle collisions will be more random. Still, it seems reasonable that a mechanism similar to that described above will be operative when gradients of ν are present. The extra stresses generated by particle overriding of the type analogous to a 'centre of dilation' will depend upon ν and $\nu_{,i}$ but perhaps only slightly upon the rate of deformation of the bulk; increased shear might increase the frequency of generation of the centres but with little change in the overall average 'stress' levels. The individual particle inertia forces associated with particle overriding are probably small compared with those associated with interparticle collisions except when grad ν is very large.

On these grounds we assume that it is permissible to neglect terms in the constitutive equation (3.14) which involve products of grad ν and $\mathbf{D}$. The argument for doing so is not a compelling one and the assumption should be regarded partially as a simplification which may require revision in view of new experimental data. Equation (3.14) then reduces to

$$\mathbf{T}^* = \mathbf{T} - \mathbf{T}_0 = a_0' \mathbf{I} + a_1 \mathbf{D}, \tag{3.25}$$

where a_0' and a_1 are functions of at most ν_0, ν, tr $\mathbf{D}$, tr $\mathbf{D}.\mathbf{D}$ and tr $\mathbf{D}.\mathbf{D}.\mathbf{D}$ or alternatively of ν_0, ν and the principal invariants

$$\left.\begin{aligned} I_1 = \operatorname{tr}\mathbf{D}, \quad I_2 = \tfrac{1}{2}(\operatorname{tr}^2\mathbf{D} - \operatorname{tr}\mathbf{D}.\mathbf{D}), \\ I_3 = \det\mathbf{D} = \tfrac{1}{6}\operatorname{tr}^3\mathbf{D} - \tfrac{1}{2}\operatorname{tr}\mathbf{D}\operatorname{tr}\mathbf{D}.\mathbf{D} + \tfrac{1}{3}\operatorname{tr}\mathbf{D}.\mathbf{D}.\mathbf{D}. \end{aligned}\right\} \tag{3.26}$$

The stress tensor $\mathbf{T}$ now consists of the sum of two parts: a dissipative part $\mathbf{T}^*$ which depends upon $\mathbf{D}$ and a second part $\mathbf{T}_0$ which is independent of $\mathbf{D}$ but which depends upon grad ν. We henceforth term $\mathbf{T}_0$ the 'ν-gradient stress' rather than the equilibrium stress. In keeping with the previous discussion of particle overriding and the fact that shear is necessary for particle overriding to occur we define

$$\mathbf{T}_0 = \lim_{\substack{\tau\to\infty \\ \mathbf{D}\to 0}} \frac{1}{\tau}\int_0^\tau \mathbf{T}\,dt,$$

where it is implied that $\mathbf{T}_0$ is averaged over a sufficient number of particles.

We now proceed to specify more completely the manner in which $\sin\phi$ and α depend upon ν. It is known from the soil-mechanics literature (e.g. Means & Parcher 1963, pp. 323–327) that the internal friction angle ϕ decreases with ν. Also, Bagnold (1966) has suspended various particles in liquid of the same density and decreased the fractional solids content ν until the residual shear resistance at zero shear rate disappeared. This concentration ν_0 at which 'fluidity' (i.e. $\phi = 0$) occurred corresponded to values of λ of around 12–14. For the present analysis, in the absence of more detailed information, we assume a simple linear relationship between $\sin\phi$ and ν as follows:

$$b = \begin{cases} \sin\phi = k(\nu - \nu_0) & \text{for} \quad \nu \geqslant \nu_0, & (3.27a) \\ 0 & \text{for} \quad \nu < \nu_0, & (3.27b) \end{cases}$$

where k is a constant chosen to give the appropriate value of ϕ at, for example, the critical void ratio.

The phenomenological coefficient α which appears in (3.13) and (3.15) is chosen to be

$$\alpha = \text{constant} \quad \text{for} \quad \nu \geqslant \nu_0 \tag{3.28a}$$

$$= 0 \quad \text{for} \quad \nu < \nu_0 \tag{3.28b}$$

in order that $\mathbf{T}_0$ be zero for concentrations less than that at which fluidity occurs. A more general dependence upon $(\nu - \nu_0)$ may be more appropriate, but with nothing further to guide us, we merely assume (3.28).

3.3. *Dissipative part of the stress tensor*

Although individual grains may behave in an elastic manner, the bulk behaves in an inelastic way during continued deformation since the grains are not connected. There is virtually no tendency for the bulk to want to return to some previous state, i.e. it has no memory (or at most an extremely short one, associated with the elastic deformation of individual grains, which we can neglect). We can consider the bulk solid to be similar to a purely viscous–inelastic, isotropic fluid, a so-called Stokesian or Reiner–Rivlin fluid (Serrin 1959; Aris 1962).

The form of the coefficients a_0' and a_1 in (3.25) should be so chosen that the expression for $\mathbf{T}$ can predict the results of Bagnold (1954) for the case of simple shear. Let us restrict attention to flows which are isochoric or approximately so (but where variations in ν are still permitted) and assume that the coefficients a_0' and a_1 depend only on the second principal invariant I_2 as well as ν and ν_0. (Note that both I_1 and I_3 are zero for isochoric, two-dimensional, fully developed channel or chute flows.) We propose that the simplest appropriate representation for the dissipative part of the stress tensor is then

$$\mathbf{T} - \mathbf{T}_0 = \mathbf{T}^* = 4\mu_0 I_2 \mathbf{I} + 4\mu_1 |I_2|^{\frac{1}{2}} \mathbf{D}, \tag{3.29}$$

where the coefficients μ_0 and μ_1 are functions of ν and tensile stresses are considered positive.

For the case of simple shear where $u_1 = u_1(x_2)$ and $u_2 = u_3 = 0$, (3.29) yields

$$T_{11}^* = T_{22}^* = T_{33}^* = -\mu_0 \left(\frac{\partial u_1}{\partial x_2}\right)^2, \tag{3.30a}$$

$$T_{12}^* = T_{21}^* = \mu_1 \left|\frac{\partial u_1}{\partial x_2}\right| \left(\frac{\partial u_1}{\partial x_2}\right), \tag{3.30b}$$

$$T_{32}^* = T_{23}^* = T_{31}^* = T_{13}^* = 0. \tag{3.30c}$$

In this case all three normal-stress components of $\mathbf{T}^*$ are equal whereas a more general form such as (3.10) could exhibit normal-stress differences. At present the experimental techniques are not developed to the extent that normal-stress effects of this kind could be distinguished.

It is seen from (3.30) that both normal and shear stresses vary as $(\partial u_1/\partial x_2)^2$ in accordance with the coaxial rotating cylinder experiments of Bagnold (1954) performed at the higher shear rates corresponding to his so-called *grain-inertia* regime. From experiments, like those of Bagnold, in which T_{22}^* and T_{12}^* are measured (and

Bulk solid	ν_∞ ($\lambda = \infty$)	ν_m	λ_m	ν_0	λ_0
Natural angular beach sand (0·318–0·414 mm)	0·644	0·555	19	0·51	12·4
Spherical lead shot (1·6 mm diameter)	0·74	0·63	18·5	—	—
Wax spheres (1·32 mm diameter)	0·74	—	—	0·60	14

TABLE 1. Values of critical fractional solids contents for various bulk solids (after Bagnold 1966).

assuming no gradients of ν) we may determine the variation of the coefficients μ_0 and μ_1 with λ or ν. For λ greater than that corresponding to fluidity, Bagnold (1966) found that the stresses increased very rapidly with ν and suggested $T^*_{22} \sim \lambda^{11}$.

For our purposes it is more convenient to express the stresses in terms of the fractional solids content ν. On the basis of Bagnold's (1954) experiments we may assume as approximations

$$\mu_0 = \beta_0 \left(\frac{\nu_\infty - \nu_0}{\nu_\infty - \nu}\right)^8, \quad \mu_1 = \beta_1 \left(\frac{\nu_\infty - \nu_0}{\nu_\infty - \nu}\right)^8 \quad \text{for} \quad \nu_0 < \nu < \nu_m, \quad (3.31), (3.32)$$

where ν_∞ corresponds to the densest possible concentration (i.e. where $\lambda = \infty$), ν_m is the maximum value of the fractional solids content at which continued shearing can occur (i.e. the ν associated with the critical voids ratio), and β_0 and β_1 are constants. Some values of ν_∞, ν_m, ν_0 and their associated values of λ quoted by Bagnold (1966) are listed in table 1.

No special significance should be attached to the particular forms of (3.31) and (3.32), they are merely convenient curve fits to Bagnold's experiments for 1·32 mm diameter wax spheres. Other analytical forms different from (3.31) and (3.32) could be used to fit the data and other sizes, shapes and materials may behave differently. Bagnold (1954) found that for $\lambda > 12$ the ratio $|T^*_{12}/T^*_{22}|$ of the shear stress to the normal stress was virtually independent of λ (and thus ν) and approximately equal to 0·4. Thus we take

$$\beta_1/\beta_0 = \text{constant} = \tan\phi_D, \quad (3.33)$$

where ϕ_D is called the dynamic internal friction angle.

The theoretical stresses for the simple-shear example (3.30) include a normal stress T^*_{33} in addition to the normal stresses T^*_{11} and T^*_{22}. Such a normal stress is expected physically on the basis of simple particle collision arguments (Bagnold 1954).

Although the accurate measurement of T^*_{33} would be a difficult experimental task, a simple experiment to indicate the presence of such a stress has been performed. A circular cylinder roughened by gluing glass beads to its surface was rotated to form a vortex flow in a mixture of glass beads and a solution of methanol and bromoform with the same density as the beads (figure 10*a*; the 3-direction is along the axis of the rotating cylinder). If the 'fluid' behaved in a Newtonian fashion then we should expect the free-surface profile gradually to decrease close to the rotating cylinder as shown in figure 10(*b*). However, when normal stress-effects are present, then we might expect that they would be evidenced by an increase in the free-surface level near the cylinder as shown. Assuming that the normal stresses in all three directions

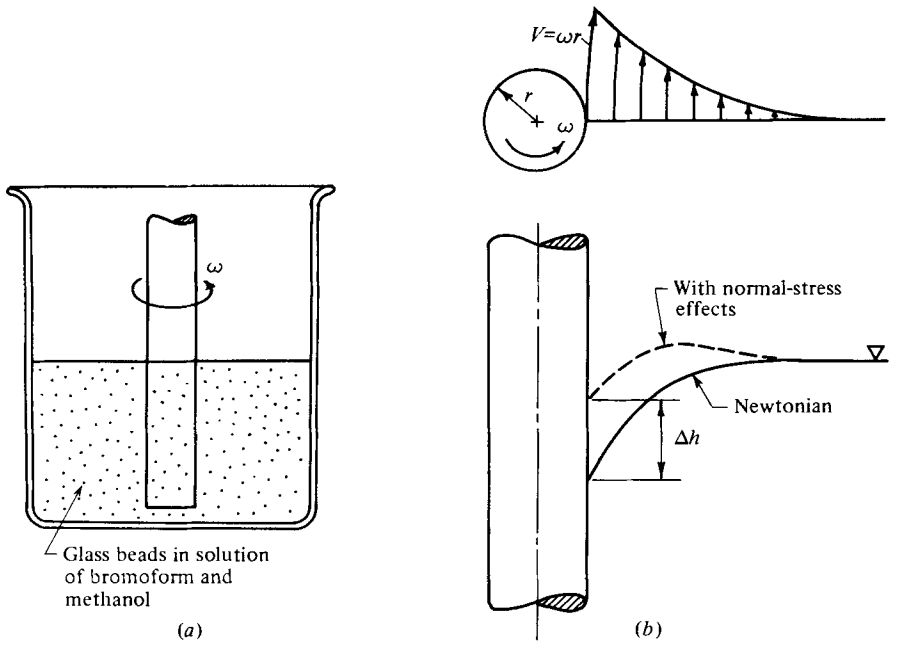

FIGURE 10. Experiment to indicate presence of normal-stress effects. (*a*) Rough cylinder rotating in beaker containing neutrally buoyant glass beads suspended in a solution of bromoform and methanol. (*b*) Anticipated velocity profile due to rotating cylinder and increase in free-surface height due to normal-stress effects. On the basis of Bagnold's (1954) experiments it is estimated that $\Delta h \simeq \frac{1}{2}$ cm assuming $\lambda \simeq 12$, $\omega \simeq 1000$ and $r \simeq 1$ cm.

are of the same order of magnitude and using Bagnold's (1954) data for $\lambda = 12$ with a cylinder radius of 1 cm and rotation rate of 1000 r.p.m., we might expect that the free-surface level should be increased above that for Newtonian behaviour by the order of $\frac{1}{2}$ cm next to the rotating cylinder. Figure 11 (plate 1) is a photograph of the experiment in operation. A bump in the free surface of the kind anticipated is evident. Some care was necessary to generate the distinct axisymmetric bump shown in the photograph. An asymmetric bump which rotated at a speed rather less than that of the rotating cylinder was more typical. Nevertheless, the presence of the normal stress T^*_{33} was apparently demonstrated.

It is worth noting also that the secondary flows evident in the inclined-chute experiments (see last part of §2) could be generated by normal-stress effects of the kind described by (3.29). It is simple to demonstrate this qualitatively. Consider flow in a rough-walled channel of finite width. Assuming a reasonable form for the first-order streamwise velocity distribution $u_1(x_2, x_3)$, the T^*_{33} stress distribution across the channel near the free surface and near the bed can be estimated from (3.29). The resulting pressure distributions are such as to generate secondary flows similar to those observed.

4. Analysis of two simple flows

The constitutive equation developed in the previous section will now be applied in the solution of two simple two-dimensional shear flows.

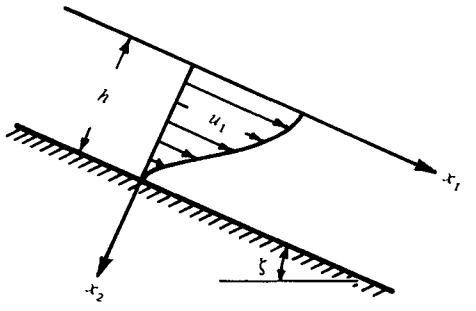

FIGURE 12. Two-dimensional gravity flow of bulk solid down a rough inclined plane.

4.1. *Flow down an inclined chute*

Consider a fully developed, two-dimensional, steady flow of a cohesionless bulk solid of constant depth h down a rough plane inclined at an angle ζ to the horizontal as shown in figure 12. Since there are no accelerations, the balance of linear momentum yields

$$-T_{12} = g \sin\zeta \int_0^{x_2} \rho \, dx_2, \tag{4.1}$$

$$-T_{22} = g \cos\zeta \int_0^{x_2} \rho \, dx_2, \tag{4.2}$$

in which $\rho = \gamma\nu$ [equation (3.1)] and

$$T_{12}/T_{22} = \tan\zeta = \text{constant}, \tag{4.3}$$

where g is the gravitational acceleration and ρ is the bulk density.

From (3.13), (3.15), (3.27), (3.29) and (3.30) we find

$$T_{12} = T_{12}^0 + T_{12}^* = \mu_1 |u_{1,2}| \, u_{1,2}, \tag{4.4}$$

$$T_{22} = T_{22}^0 + T_{22}^* = -\alpha(b^{-1}+1)\, \nu_{,2}\, \nu_{,2} - \mu_0 (u_{1,2})^2. \tag{4.5}$$

For the case to be studied $u_{1,2}$ is always negative, thus we can write

$$T_{12} = -\mu_1 (u_{1,2})^2. \tag{4.6}$$

Combining (4.3), (4.5), (4.6) and (3.33) yields

$$\alpha \left(\frac{1}{b}+1\right) (\nu_{,2})^2 = -\left(\frac{1}{\tan\zeta} - \frac{1}{\tan\phi_D}\right) T_{12}. \tag{4.7}$$

Note that ζ must be greater than the angle of repose ϕ_R for flow to occur on a rough plane but must be less than the dynamic internal friction angle ϕ_D, otherwise the flow accelerates; thus for steady, fully developed, constant depth flow

$$\phi_R < \zeta < \phi_D. \tag{4.8}$$

The variation of ρ over this depth is small and we can approximate the integrals in (4.1) and (4.2) as

$$\int_0^{x_2} \rho \, dx_2 \cong \bar{\rho} x_2 = \gamma \bar{\nu} x_2, \tag{4.9}$$

where $\bar{\rho}$ and $\bar{\nu}$ are average values of ρ and ν over the depth h.

By making use of (3.28), (4.1) and (4.9) we may put (4.7) in the form

$$\alpha\left[\frac{1+k(\nu-\nu_0)}{k(\nu-\nu_0)}\right](\nu_{,2})^2 = \Gamma x_2, \tag{4.10}$$

where
$$\Gamma = g\gamma\bar{\nu}\sin\zeta(1/\tan\zeta - 1/\tan\phi_D) = \text{constant}. \tag{4.11}$$

The fractional solids content varies only slightly over the depth, at most between ν_m and ν_0, and we approximate (4.10) as

$$(\nu-\nu_0)^{-\frac{1}{2}}\nu_{,2} = \pm\left(\frac{\Gamma}{M}x_2\right)^{\frac{1}{2}}, \tag{4.12}$$

where
$$M = \alpha\left[\frac{1+k(\bar{\nu}-\nu_0)}{k}\right] = \text{constant}. \tag{4.13}$$

Equation (4.12) may be integrated for cases in which ν either decreases or increases with depth x_2. Only the latter case ($\nu_{,2}$ positive) will be discussed here, in conformity with the situation evident in the present experiments (see §6). In this case (4.12) yields

$$(\nu-\nu_0)^{\frac{1}{2}} = \frac{1}{3}\left(\frac{\Gamma}{M}\right)^{\frac{1}{2}}x_2^{\frac{3}{2}} + C, \tag{4.14}$$

where the constant C is zero if $\nu = \nu_0$ at the free surface $x_2 = 0$.

Note that since $\alpha = 0$ for $\nu \leqslant \nu_0$, (4.5), (4.6) and (3.33) yield

$$T_{12}/T_{22} = \tan\phi_D \quad \text{for} \quad \nu \leqslant \nu_0. \tag{4.15}$$

Since in general for steady flow $T_{12}/T_{22} = \tan\zeta$,

(4.15) implies that steady fully developed flows are not possible for situations when $\nu < \nu_0$ and the channel inclination $\zeta < \phi_D$. Thus in taking $\nu = \nu_0$ at the free surface we are assuming that the flow adapts to the lowest concentration consistent with a fully developed flow.

Because there is a maximum value of the fractional solids content ν_m at which continued shearing can occur, (4.14) provides the maximum flow depth possible for fully developed flow:

$$h_m = \left[3\left(\frac{M}{\Gamma}\right)^{\frac{1}{2}}(\nu_m-\nu_0)^{\frac{1}{2}}\right]^{\frac{2}{3}}. \tag{4.16}$$

From (4.14) the distribution of ν over the depth may be expressed approximately as

$$\frac{\nu-\nu_0}{\nu_b-\nu_0} = \left[\frac{x_2}{h}\right]^3, \tag{4.17}$$

where h is the uniform depth of flow and ν_b is the fractional solids content at the channel bed.

In order to determine the velocity profile, (3.32), (4.1), (4.6) and (4.9) may be combined in the form

$$\frac{du_1}{dx_2} = -\left(\frac{g\bar{\nu}\gamma\sin\zeta}{\beta_{12}}\right)^{\frac{1}{2}}\left[\frac{\nu_\infty-\nu}{\nu_\infty-\nu_0}\right]^4 x_2^{\frac{1}{2}}. \tag{4.18}$$

Using the approximation (4.17), (4.18) may then be put in the form

$$du_1 = \frac{-2}{3}\left(\frac{g\bar{\nu}\gamma\sin\zeta}{\beta_{12}}\right)^{\frac{1}{2}}h^{\frac{3}{2}}[1-Ny^2]^4\,dy, \tag{4.19}$$

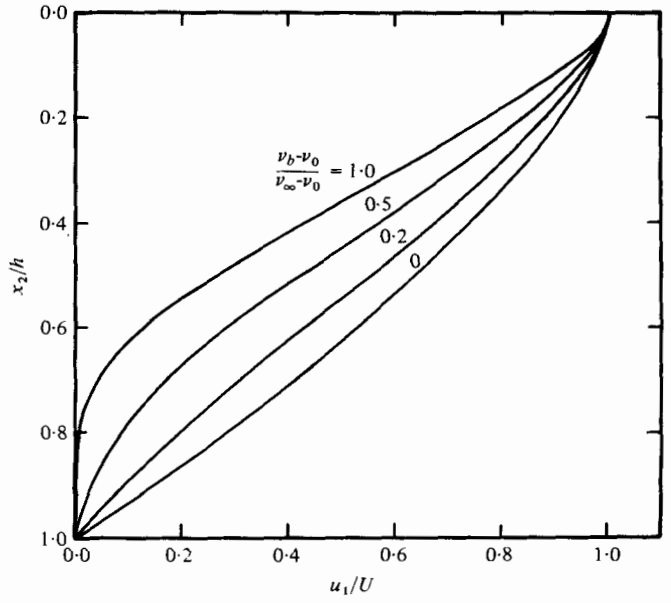

FIGURE 13. Theoretical non-dimensional velocity profiles for two-dimensional flow down a rough inclined plane.

where $N = (\nu_b - \nu_0)/(\nu_\infty - \nu_0)$ and $y = (x_2/h)^{\frac{3}{2}}$. Integrating (4.19) and taking the bed to be so rough that the no-slip condition applies there, we obtain

$$u_1 = \frac{2}{3}\left(\frac{g\bar{\nu}\gamma \sin\zeta}{\beta_{12}}\right)^{\frac{1}{2}} h^{\frac{3}{2}} \sum_{j=0}^{4} \frac{{}_4C_j(-N)^j}{(2j+1)}\,[1-y^{2j+1}], \tag{4.20}$$

where the ${}_4C_j$ are the binomial coefficients ${}_rC_j$ for $r = 4$.

It should be emphasized that, if the bed is sufficiently smooth that the angle of friction between the bed and the bulk solid is less than the angle of internal friction, slip occurs and slug-type flow results.

The non-dimensional velocity profiles, given by

$$\frac{u_1}{U} = \sum_{j=0}^{4} P_j[1-y^{2j+1}] \Big/ \sum_{j=0}^{4} P_j, \tag{4.21}$$

where

$$P_j = {}_4C_j(-N)^j/(2j+1) \tag{4.22}$$

and U is the surface velocity, are shown in figure 13 for various values of the parameter N. Although curves are shown for $0 < N < 1$, the maximum possible value for N is less than unity since $\nu_m < \nu_\infty$.

From (4.14) it can be shown that

$$N \sim \Gamma \sim \sin\zeta(1/\tan\zeta - 1/\tan\phi_D). \tag{4.23}$$

Thus if the chute inclination ζ is ϕ_D, then $N = 0$, the concentration is uniform, $\nu = \nu_0$ and the velocity profile has the form

$$u_1/U = 1-(x_2/h)^{\frac{3}{2}}. \tag{4.24}$$

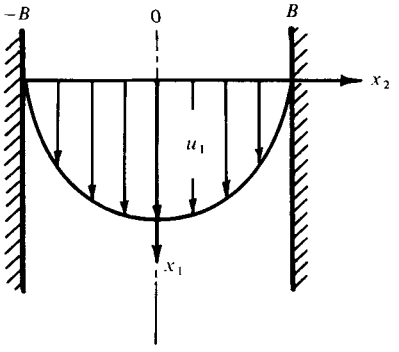

FIGURE 14. Two-dimensional gravity flow of a bulk solid down a rough-walled vertical channel.

As ζ is decreased from ϕ_D to ϕ_R (the minimum value for fully developed flow), the variation in density over the depth increases and the velocity profiles become less full and eventually develop a shape with an inflexion point somewhat reminiscent of a laminar boundary layer near separation. The physical explanation of this behaviour is evident from (4.1), (4.6) and (3.32). The shear stress T_{12} varies almost linearly with x_2 for all inclinations ζ. Since μ_1 is so sensitive to variations in ν, a slight increase in ν near the bed reduces the shear rate $u_{1,2}$ required there for the equilibrium of forces.

Note that from (4.20), (4.14) and (4.13) the surface velocity U can be shown to depend upon α. Thus, in principle, the coefficient α could be determined from experiments of flow down inclined chutes if β_1 and k were known from other experiments such as those of Bagnold (1954).

4.2. *Flow in a vertical channel*

An analysis similar to that in the previous subsection can be performed for the fully developed two-dimensional flow of a cohesionless bulk solid in a rough-walled vertical channel of width $2B$ as shown in figure 14. The balance of linear momentum yields

$$T_{12} = -\int_0^{x_2} \rho g \, dx_2, \tag{4.25}$$

$$T_{22} = \text{constant} = -A. \tag{4.26}$$

Using the constitutive relations (4.5) and (4.6) gives the approximation

$$\alpha(b^{-1}+1)(\nu_{,2})^2 = A - (\mu_0/\mu_1)\bar{\rho} g x_2 \quad \text{for} \quad x_2 > 0 \tag{4.27}$$

and

$$(u_{1,2})^2 = \mu_1^{-1}\gamma\bar{\nu} g x_2 \quad \text{for} \quad x_2 > 0. \tag{4.28}$$

Using approximations similar to those used to derive (4.12), we may put (4.27) in the following form:

$$(\nu - \nu_0)^{-\frac{1}{2}}\nu_{,2} = \pm\left(\frac{1}{M}\right)^{\frac{1}{2}}\left(A - \frac{\beta_0}{\beta_1}\bar{\rho} g x_2\right)^{\frac{1}{2}}. \tag{4.29}$$

If we take $\nu = \nu_0$ at the wall $x_2 = B$ and $\nu_{,2}$ positive then (4.29) may be integrated to yield

$$(\nu - \nu_0)^{\frac{1}{2}} = \frac{1}{3}\left[\frac{\beta_0 g\bar{\rho}}{M\beta_1}\right]^{\frac{1}{2}} B^{\frac{3}{2}}\left[1 - \frac{x_2}{B}\right]^{\frac{3}{2}} \quad \text{for} \quad x_2 > 0. \tag{4.30}$$

Here the fractional solids content ν is a maximum at the centre-line of the channel and decreases to ν_0 at the walls. There is a maximum possible value of the channel half-width B for which there is no plug-flow region. This maximum value $B_{\max}$ corresponds to the case when the fractional solids content ν_c at the centre-line is equal to ν_m.

Substituting (3.32) into (4.28) yields

$$\frac{du_1}{dx_2} = -\left(\frac{g\bar{\rho}}{\beta_1}\right)^{\frac{1}{2}}\left[1-\left(\frac{\nu_c-\nu_0}{\nu_\infty-\nu_0}\right)\left(\frac{\nu-\nu_0}{\nu_c-\nu_0}\right)\right]^4\sqrt{x_2} \quad \text{for} \quad x_2 > 0. \tag{4.31}$$

From (4.30) we obtain

$$\left[\frac{\nu-\nu_0}{\nu_c-\nu_0}\right] = \left[1-\frac{x_2}{B}\right]^3. \tag{4.32}$$

By using (4.32), we may put (4.31) in the form

$$du_1 = -2\left(\frac{g\bar{\rho}}{\beta_1}\right)^{\frac{1}{2}}[1-R(1-z^2)^3]^4 B^{\frac{3}{2}} z^2 dz \quad \text{for} \quad x_2 > 0, \tag{4.33}$$

where $R = (\nu_c-\nu_0)/(\nu_\infty-\nu_0)$ and $z = (x_2/B)^{\frac{1}{2}}$. Integrating (4.33) and applying the no-slip condition at the wall yields

$$u_1 = 2B^{\frac{3}{2}}\left(\frac{g\bar{\rho}}{\beta_1}\right)^{\frac{1}{2}}\sum_{j=0}^{4} {}_4C_j(-R)^j \sum_{k=0}^{3j} {}_{3j}C_k(-1)^k \frac{(1-z^{2k+3})}{(2k+3)}. \tag{4.34}$$

Dividing (4.34) by the velocity U at the centre-line gives the non-dimensional velocity profile:

$$\frac{u_1}{U} = \frac{\sum_{j=0}^{4} {}_4C_j(-R)^j \sum_{k=0}^{3j} {}_{3j}C_k(-1)^k \frac{(1-z^{2k+3})}{(2k+3)}}{\sum_{j=0}^{4} {}_4C_j(-R)^j \sum_{k=0}^{3j} {}_{3j}C_k(-1)^k \frac{1}{(2k+3)}}, \tag{4.35}$$

which is shown in figure 15 for various values of the parameter R.

For the case $R = 0$, the fractional solids content ν is ν_0 throughout and the velocity profile is given by

$$u_1/U = 1-(x_2/B)^{\frac{3}{2}}, \tag{4.36}$$

which is the same form as that for inclined-chute flow when $N = 0$. With increasing R the concentration increases in the central portion of the channel and the velocity profile becomes more blunted.

5. Apparatus and experimental procedure for inclined-chute and vertical-channel flows

Experiments were performed in an attempt to investigate some features of the two-dimensional shear flows studied theoretically in the previous section. Velocity profiles at various streamwise stations were measured for both the vertical-channel and the inclined-chute flow. The variation of depth with streamwise distance was measured for the inclined-chute flow.

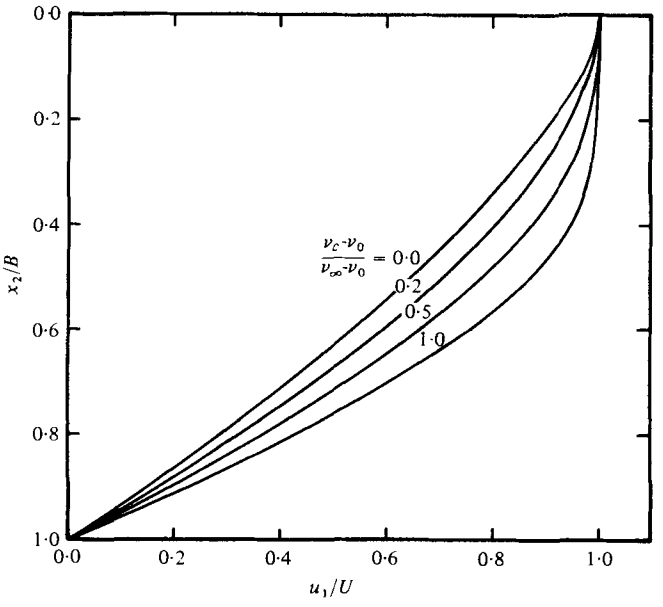

FIGURE 15. Theoretical non-dimensional velocity profiles for two-dimensional flow down a rough-walled vertical channel.

5.1. *Flow material, test section and material handling equipment*

The bulk solid used as the flow material was composed of spherical polystyrene beads (figure 16*a*, plate 2) with a specific gravity of 1·03. Figure 16(*b*) (plate 2) shows the particle size distribution; the mean diameter was approximately 1·2 mm.

The experimental rig was designed such that both the inclined-chute and the vertical-channel tests could be performed with the same basic apparatus, which is shown schematically in figure 17. The beads were stored in the upper supply bin. A sheet–steel hopper in the form of an inverted pyramid was attached to the top, plywood part of the bin, which has a cross-section of 0·8 × 0·8 m. Since the flow rate of granular materials through orifices is independent of the head for heads greater than a few times the orifice dimensions (Brown & Richards 1970, p. 167), the bin provided a constant discharge for almost all of the granular material which it contained. The test section was bolted directly to a flange on the bottom of the hopper for the vertical-channel tests. Plates with circular orifices of various diameters could be inserted at the bottom of the vertical channel to control the flow rate. An adjustable angled Perspex transition section, which connected the test section to the hopper, was used in the inclined-chute tests. Various gates could be fixed in the transition section to control the flow rate and upstream flow depths. After flow through the test section, the beads went either directly (for the vertical-channel test) or through an inclined pipe (for the inclined-chute test) to the 40 gallon collector drum. After the supply bin had emptied, the collector drum was capped and the polystyrene beads were transported pneumatically through a spiral plastic pipe (5 cm diameter) up again to the supply bin.

Two of the side walls of the 1·22 m long test section were smooth glass to permit slip of the bulk solid as well as to enable flow visualization. The other two side walls

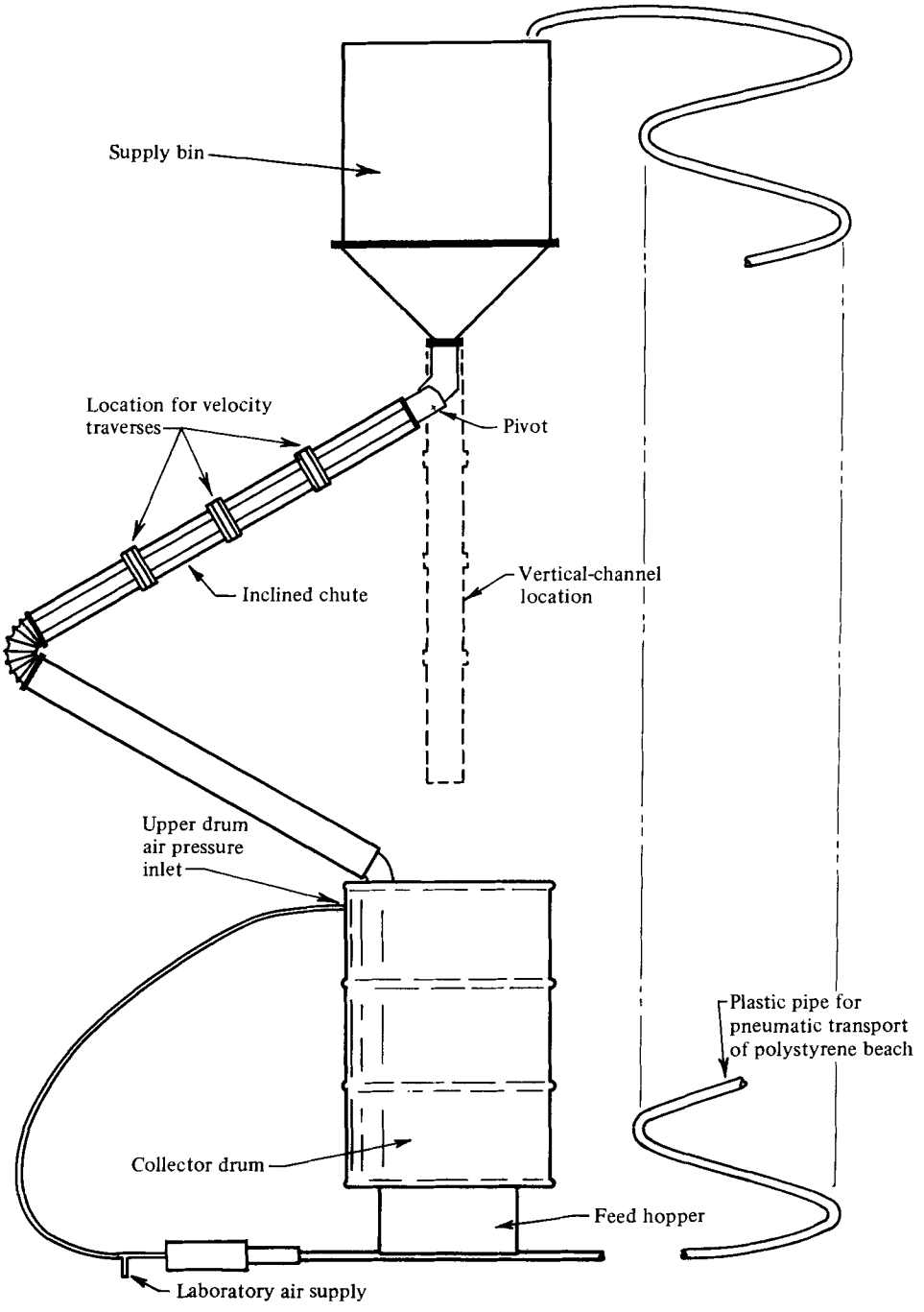

FIGURE 17. Schematic diagram of inclined-chute and vertical-channel apparatus.

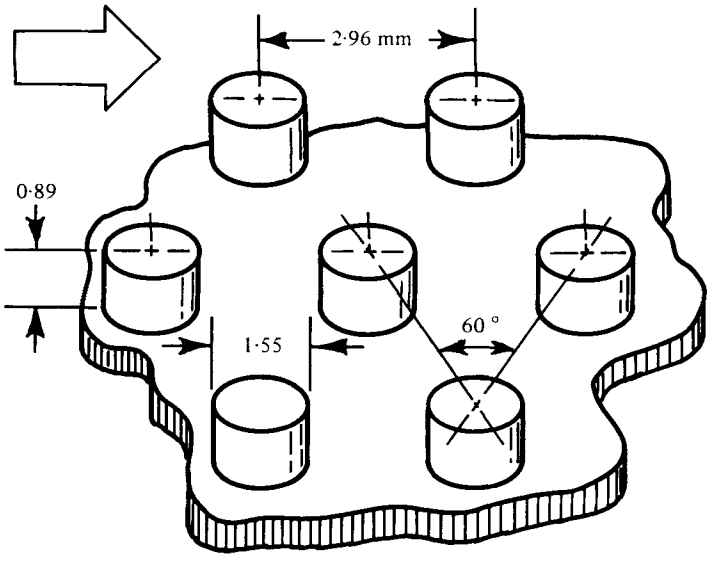

FIGURE 18. Geometry of rubber-sheet wall roughness.

were made from an aluminium channel faced with rough rubber sheets to maintain a no-slip condition. The overall objective was to generate a two-dimensional shear flow. Figure 18 illustrates the rubber wall roughness, which is similar to that used on some table tennis bats. The test section was rectangular in cross-section, 3·86 cm between the two glass walls and 3·46 cm between the tops of the roughness elements on the roughened aluminium walls.

Provisions were made at three streamwise stations (33, 63·5 and 94 cm from the test-section entry) to accommodate the transversing gear for measurement of the velocity profiles.

5.2. *Instrumentation*

The method of measuring velocity profiles by analysing ciné films of the flow described in § 2 was not very suitable for the more turbulent shear flows and a better way which could automatically average the velocity fluctuation over at least a few seconds was required. A technique was devised which makes use of two fibre optic probes set a small distance apart in the streamwise direction (see figures 19 and 20). The probes were mounted in a traversing probe holder with the axis of each probe perpendicular to the glass side walls. A dial gauge was used to record the position of the probes during the traverse.

The MTI KD-P065R 'Fotonic fibre optic probes' were used in combination with MTI KD-C2S 'cartridges' and MTI KD-45 'Fotonic control units'; all are manufactured by Mechanical Technology Incorporated of Latham, N.Y.

The probes contain a bundle of optical fibres, of which about half transmit light from a source in the cartridge and half act as receivers. The probes are normally used as displacement transducers and operate by detecting the intensity of light reflected from a nearby surface. The output of each unit depends upon the proximity of a light-reflecting surface to the tip of the probe. A typical calibration curve is shown in figure 21. In order that we operated on that portion of the calibration where output de-

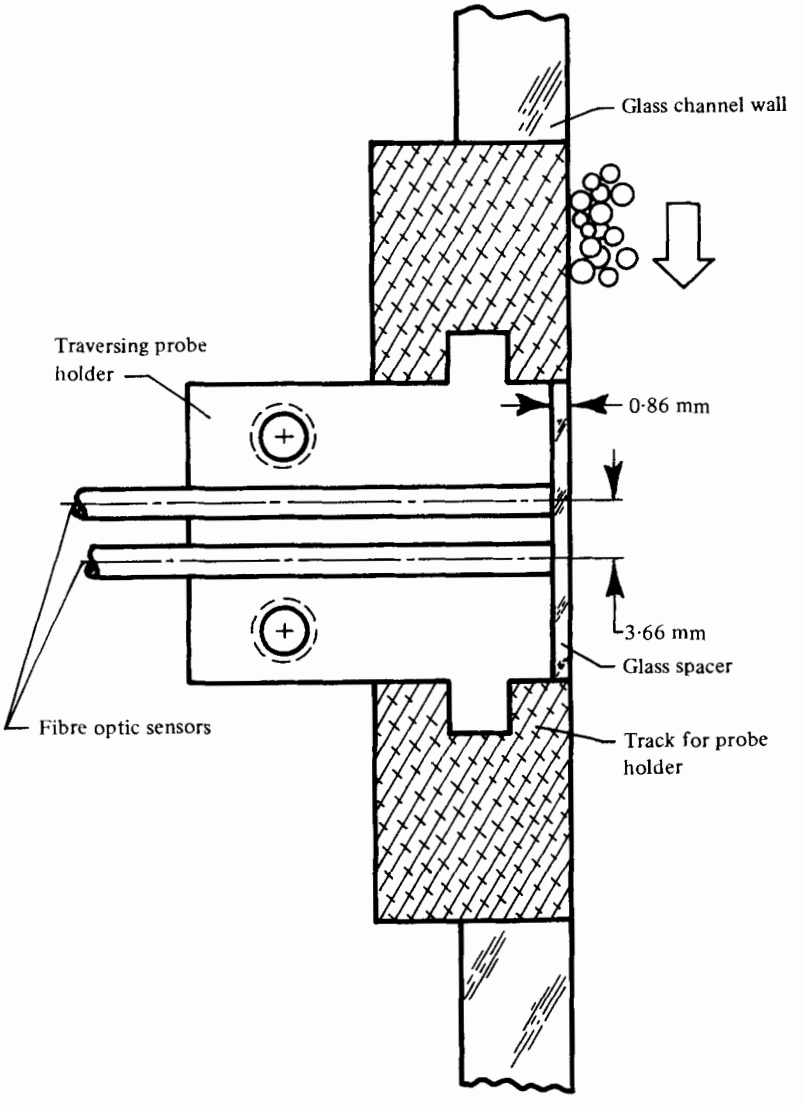

FIGURE 19. Arrangement of fibre optic sensors for bulk solids velocity measurement.

creases with distance, a glass spacer plate 0·86 mm thick was used between the end of the probes and the flowing beads (figure 19). Thus the passage of a single particle past one of the sensors generated a pulse-like output. Flow of a mass of beads generates a fluctuating signal from the upstream sensor and a similar, but time-delayed, signal from the second sensor. By cross-correlating the two sensor outputs, the transit time between the two probes and thus the mean velocity can be determined. A Princeton Applied Research model 100A correlator was used to obtain the cross-correlation function, which was displayed on a Tektronix 502 oscilloscope. A typical oscillogram of the cross-correlation function taken during the inclined-chute tests is shown in figure 22 (plate 3). A second Tektronix 502 oscilloscope was used to monitor the Fotonic sensor signals (figure 20).

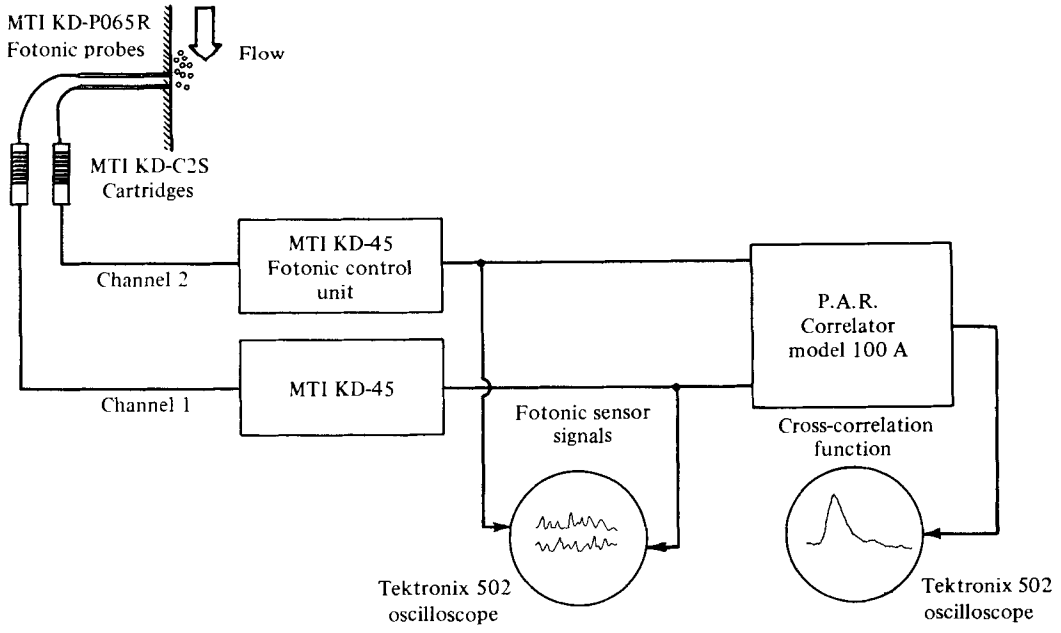

FIGURE 20. Block diagram of circuit for velocity measurement using fibre optic sensors.

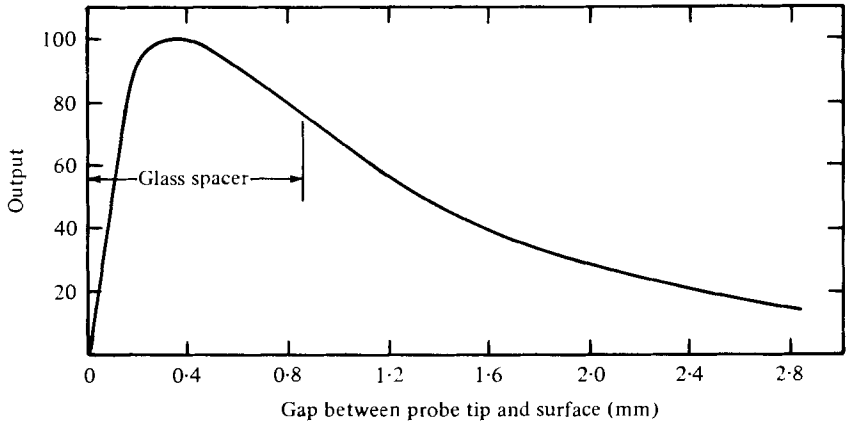

FIGURE 21. Typical fibre optic probe calibration.

Preliminary tests with this technique showed that the optimum spacing between the probes was between 2 and 4 mm for the polystyrene beads used in these tests. Since the transmitting and receiving fibres are distributed randomly in the bundle making up the Fotonic probe it was necessary to perform calibration tests to determine the effective separation distance between the two probes mounted in the traversing probe holder (figure 19). A variable-speed d.c. motor was used to rotate a large 'dish' containing beads. With the probes mounted above the beads when they were moving by at a known velocity, the effective separation distance was obtained from the measured cross-correlation function. The effective separation distance of 3·66 mm agreed closely with the measured distance between the geometric axes of the probes.

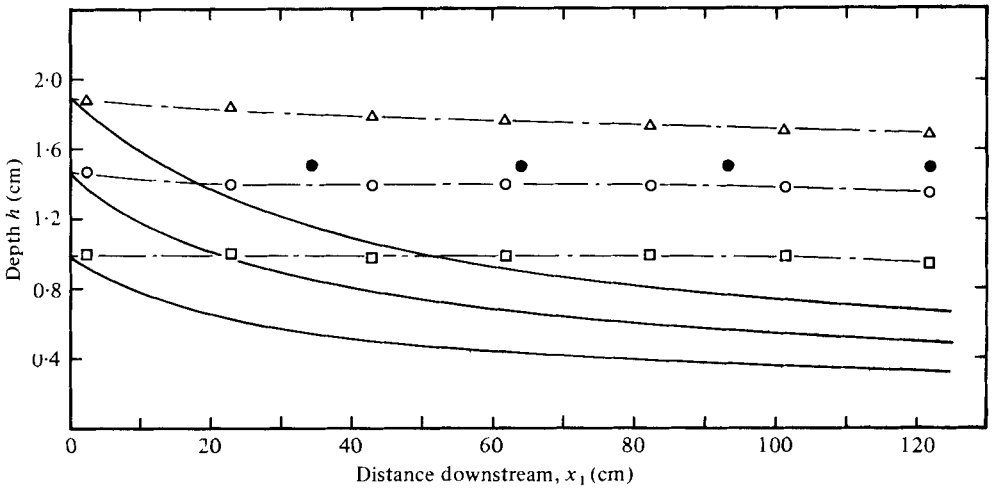

FIGURE 23. Comparison of experimental depth profiles with Roberts' (1969) theory. Rough bottom wall, $\zeta = 32{\cdot}6°$. □, ○, △, mass flow rates of 45·5, 88·2, and 129·8 g/s respectively; open symbols, visual readings during each run; solid symbols, depths estimated from photographs of free surface. ——, Roberts' theory for $\mu = 0{\cdot}453$ and $k = 0{\cdot}453$.

6. Experimental measurements of developed flows

6.1. *Flow in inclined chutes*

6.1.1. *Depth profiles.* Streamwise depth profiles were measured for several bed inclinations ζ. Although flow occurred for bed slopes as low as $\zeta = 25°$, only a surface layer was in motion. A wedge-shaped dead zone existed below the surface layer such that the inclination of the 'free' surface was about 26·5°. Because of friction on the vertical glass side walls, the free-surface slopes at which motion occurred was slightly larger than the angle of repose of the polystyrene beads ($\phi_R \simeq 24°$). By a bed slope of about 29° the dead zone had disappeared and the depth profiles tended to become more uniform.

Figure 23 shows observed depth profiles for three mass flow rates corresponding to three different upstream gate openings at a bed slope $\zeta = 32{\cdot}6°$. Because of the turbulent saltating motion of individual particles a low density surface layer existed. The 'free surface' was therefore not distinct and it was difficult to estimate accurately the flow depth from visual observations. The open symbols in figure 23 were obtained during the test runs from sightings on scales glued to the glass side wall. Still photographs of the surface at various streamwise stations were also taken using an electronic flash unit. It was possible to estimate the mean 'free surface' from these still photographs, accounting for the low density surface cloud of saltating particles. The depths estimated from the photographs were slightly larger than those estimated visually during flow (figure 23).

The profiles shown in figure 23 for the two lower flow rates reach a uniform depth in a relatively short distance. This behaviour is in accord with that of the preliminary experiments performed with quite different apparatus and materials (§2.2).

Depth profiles were also calculated using Roberts' (1969) theory. This theory makes use of an equivalent coefficient of friction μ_E between the flowing beads and the bed

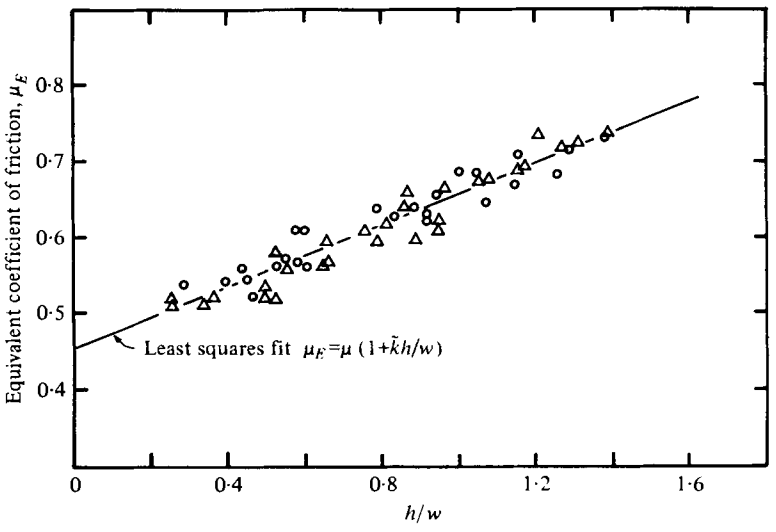

FIGURE 24. Determination of frictional parameters for Roberts' (1969) theory. Tests with polystyrene beads in chute with rough bottom and glass side walls. △, ○, carts of 1·5 and 3·3 g respectively. Least-squares fit to data yields $\mu = 0{\cdot}453$ and $\tilde{k} = 0{\cdot}453$.

and wide walls of the chute. Roberts expressed μ_E as a linear function of the material depth-to-width ratio h/w:

$$\mu_E = \mu(1 + \tilde{k}\,h/w). \tag{6.1}$$

Following Roberts (1969), μ_E was determined by measuring the angle of repose for beads present in the chute and retained between the two end plates of carts which moved freely in the chute and rested on runners fixed to the top of the glass side walls. Corrections were applied to account for the cart weight and runner friction. The carts were made from thin balsa-wood sheets in order to be as light as possible (1·5 g and 3·3 g) and the corrections to μ_E were small (at most 2 % for the 1·5 g cart and 6 % for the 3·3 g cart). Figure 24 shows the results of these tests. A linear least-squares fit to these data determined that $\mu = 0{\cdot}453$ and $\tilde{k} = 0{\cdot}453$. The measured mass flow rates, initial flow depths and an estimated bulk density $\bar{\rho} = 0{\cdot}58$ g/c.c. were used to estimate the initial mean flow velocity. The depth profiles predicted by Roberts' theory (figure 23) continually decrease with distance and fall below the measured depths.

Depth profiles were also measured for slightly higher bed inclination angles: $\zeta = 35{\cdot}3°$ and $39{\cdot}3°$. For these values of ζ, Roberts' theory again predicted accelerating flows whose depths were considerably below the measured depths. The experimental flows approached uniform depth with downstream distance. At higher bed slopes, the experimental flows were found to accelerate over the length of the chute, conforming more closely to the predictions of Roberts. This behaviour is in accord with the analysis in §4, which suggested that fully developed, constant depth flows could exist for only a limited range of bed slopes, $\phi_R < \zeta < \phi_D$.

6.1.2. *Velocity profiles.* Detailed velocity measurements were made for several angles of inclination ζ where the flows appeared to be well developed, with little variation of the depth and velocity profile in the streamwise direction. Figures 25–27 show the velocity profiles at three streamwise stations for $\zeta = 32{\cdot}6°$, $35{\cdot}3°$ and $39{\cdot}3°$. Note that points which lie above the mean 'free surface' have been recorded. The

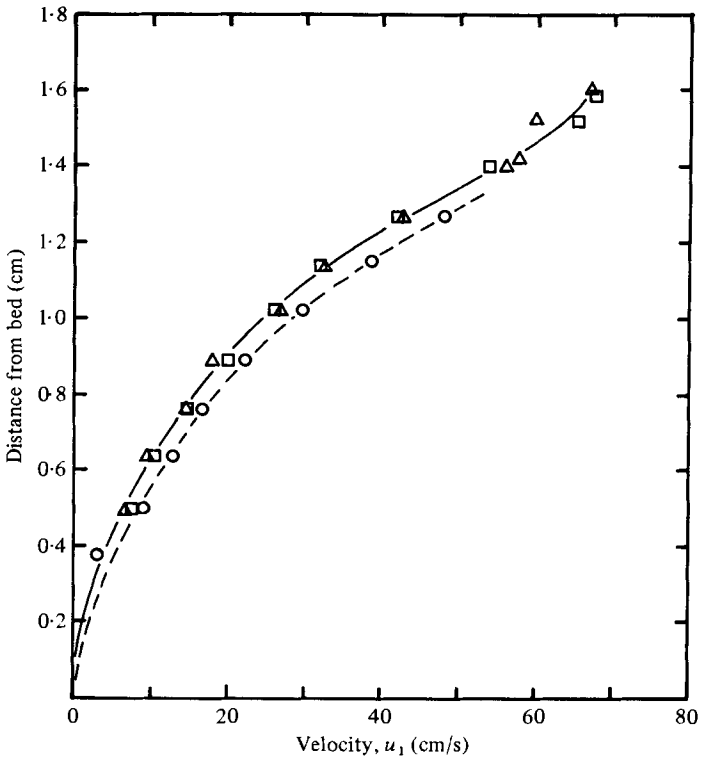

FIGURE 25. Velocity profiles for flow down inclined chute at a mass flow rate of 88·2 g/s and ζ = 32·6°. ○, △, □, streamwise stations 33·0, 63·5 and 94·0 cm respectively from entry.

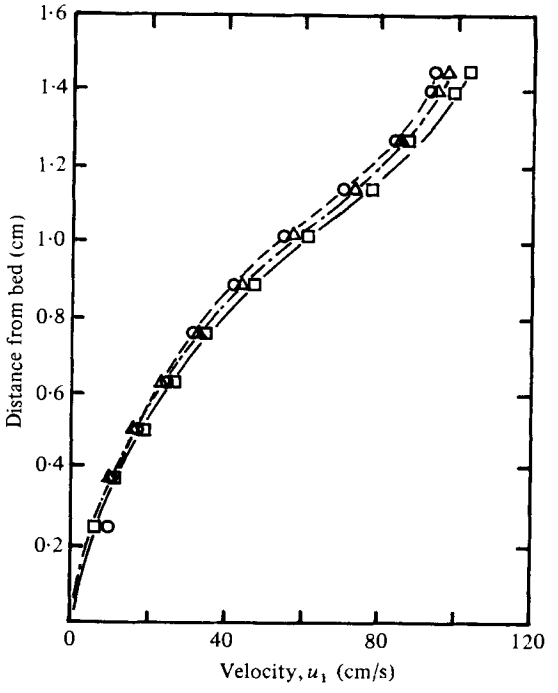

FIGURE 26. Velocity profiles for flow down inclined chute at a mass flow rate of 108·7 g/s and ζ = 35·3°. ○, △, □, streamwise stations 33·0, 63·5 and 94·0 cm respectively from entry.

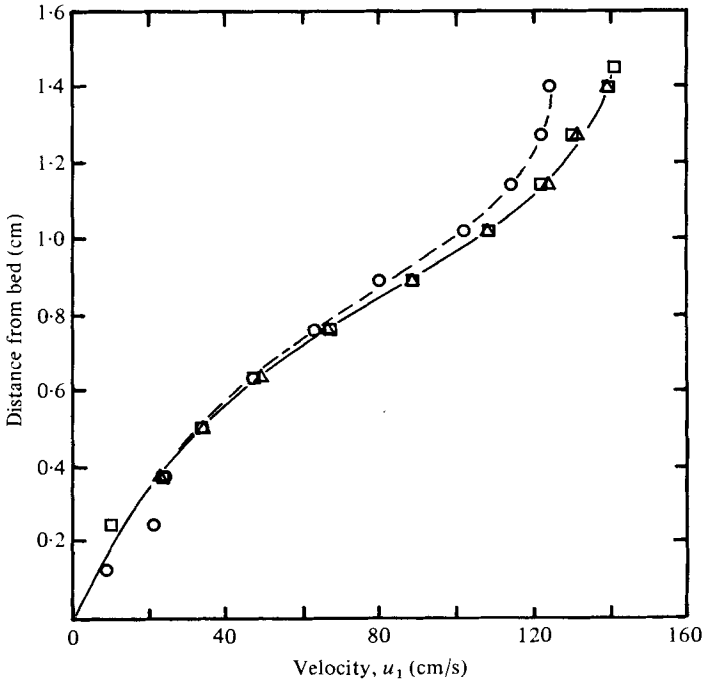

FIGURE 27. Velocity profiles for flow down inclined chute at a mass flow rate of 132·6 g/s and $\zeta = 39{\cdot}3°$. ○, △, □, streamwise stations 33·0, 63·5 and 94·0 cm respectively from entry.

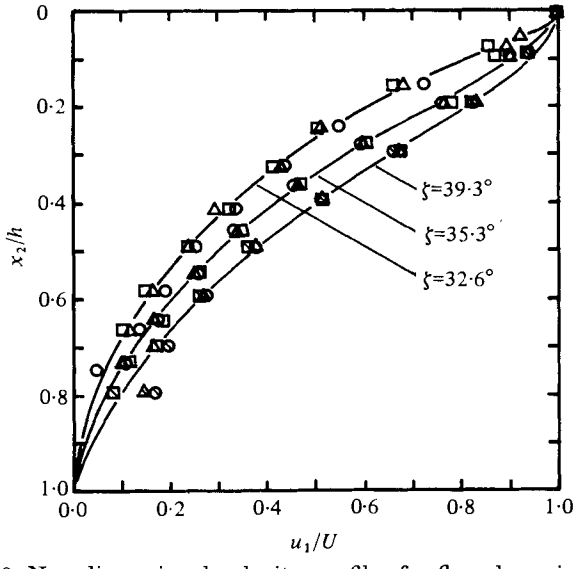

FIGURE 28. Non-dimensional velocity profiles for flow down inclined chute. ○, △, □, streamwise stations 33·0, 63·5 and 94·0 cm respectively from entry.

ζ (deg)	x_1 (cm)	h (cm)	U (cm/s)	M_c (g/s)	M_m (g/s)	M_c/M_m
32·6	33·0	1·5	66·5	69·3	88·2	0·786
	63·5		63·0			
	94·0		63·0			
35·3	33·0	1·4	93	116	108·7	1·07
	63·5		95			
	94·0		100			
39·3	33·0	1·25	122	155	132·6	1·17
	63·5		131			
	94·0		131			

TABLE 2. Parameters associated with measurements of inclined-chute velocity profiles.

instrumentation senses saltating particles in the low density surface cloud, even though their passage past the probes may be infrequent. The experimental velocity profiles with an inflexion point are similar in shape to the theoretical predictions of §4.1 (see figure 13).

The velocity profiles were replotted (figure 28) in non-dimensional form, u_1/U *vs.* x_2/h, using values of h and U associated with the mean 'free surface' determined from the still photographs (see table 2). With increasing ζ the profiles become more full as anticipated from the analysis in §4.1.

The mass flow rates M_m were measured for each run and the mean value for each chute inclination is listed in table 2. Assuming the flow to be two-dimensional and of width w, the mass flow rate can be calculated from the velocity profile as follows:

$$M_c = w \int_0^h \rho u_1 dx_2,$$

or

$$M_c \simeq w\bar{\rho} U h \int_0^1 \frac{u_1}{U} d\left(\frac{x_2}{h}\right). \tag{6.2}$$

With $w = 3{\cdot}86$ cm, $\bar{\rho}$ estimated as 0·58 g/c.c., h and U as listed in table 2, and the integral in (6.2) evaluated from figure 28, mean values of M_c for each chute inclination were determined and are shown in table 2.

The ratios of M_c to M_m for the three values of ζ are also given in table 2. Considerable uncertainty exists in the calculated mass flow rate M_c because of the uncertainties in both $\bar{\rho}$ and h. The value of 0·58 g/c.c. for $\bar{\rho}$ is only an educated guess. A slight change in the choice for h unfortunately results in a large difference in M_c.

For $\zeta = 32{\cdot}6°$, $M_c/M_m = 0{\cdot}786$, i.e. quite a bit less than one. Since it is unlikely that $\bar{\rho}$ is much greater than 0·58 g/c.c. and h much larger than 1·5 cm, it appears most probable that here the flow was not two-dimensional. The friction between the vertical glass side walls and the adjacent beads not only retarded the flow but probably caused a three-dimensional flow to develop accordingly.

For $\zeta = 35{\cdot}3°$ and $39{\cdot}3°$, the values of M_c/M_m are both somewhat larger than one, and hence a two-dimensional flow appears more likely. Slight reductions in the estimates of $\bar{\rho}$ and h could bring M_c/M_m to unity.

In the tests, friction arose between the flowing beads and the vertical glass side

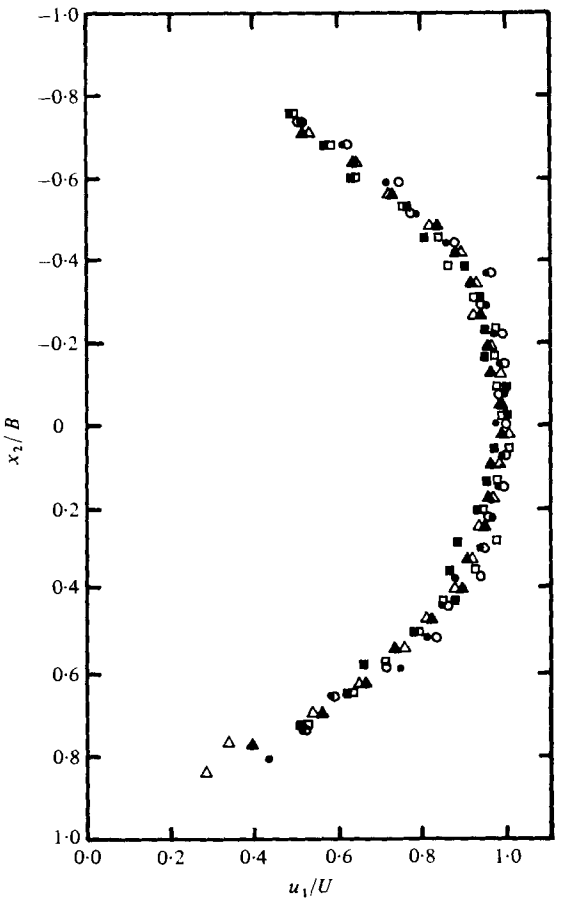

FIGURE 29. Experimental non-dimensional velocity prolfie in vertical channel at a mass flow rate of 93·1 g/s. ○, △, □, streamwise stations of 33·0, 63·5, and 94·0 cm respectively from entry. Open and solid symbols distinguish two different runs.

walls. Since this side-wall friction was not considered in the analysis of §4.1, direct comparisons between figures 13 and 28 are not appropriate. However, the general trends of the analysis seem to be verified.

6.2. *Flow in vertical channels*

The same test section as was used in the inclined-chute tests was mounted in the vertical position and flow control orifice plates were installed at the lower end of the channel. Orifice diameters of 1·27, 1·91 and 2·54 cm were found to give mass flow rates of 12·1, 42·2 and 93·1 g/s respectively.

6.2.1. *Velocity profiles.* Velocity profiles were measured at three streamwise stations, 33, 63·5 and 94 cm from the entry, for the three mass flow rates. The velocity profiles were found to be fully developed and similar at all three stations for each of the three mass flow rates. The non-dimensional profiles, u_1/U *vs.* x_2/B, for a mass flow rate of 93·1 g/s are shown in figure 29. The data show little scatter and good reproducibility. The velocity approaches zero at the two rough side walls ($x_2/B = \pm 1$). The experi-

M_m (g/s)	U (cm/s)	M_c (g/s)	M_c/M_m
12·1	1·30	6·99	0·578
42·2	4·43	23·8	0·564
93·1	9·54	51·3	0·538

TABLE 3. Vertical-channel mass flow rates.

mental velocity profiles for the two lower mass flow rates were virtually identical to those of figure 29 and are not shown for this reason.

If we assume that $\nu_\infty = 0{\cdot}74\,(\lambda = \infty)$, $\nu_0 = 0{\cdot}58\,(\lambda = 12)$ and the centre-line concentration corresponds to the critical voids ratio $\nu_c = \nu_m = 0{\cdot}63\,(\lambda = 19)$, then the parameter $R = (\nu_c - \nu_0)/(\nu_\infty - \nu_0) \simeq 0{\cdot}3$. It is found that the theoretical velocity profile in figure 15 for $R = 0{\cdot}3$ is close to the experimental one shown in figure 29. This similarity is perhaps fortuitous since it was found by direct measurement of the mass flow that the velocity profiles were not two-dimensional as in the theory. Table 3 compares M_m, the mass flow rate measured directly, with M_c, the mass flow rate determined from the wall velocity profile (figure 29) assuming a two-dimensional flow and $\bar{\rho} = 0{\cdot}58$ (similar to the procedure followed in §6.1.2).† The ratio M_c/M_m varied from 0·538 to 0·578, indicating very large departures from the assumed two-dimensional flow. The effects of the friction on the glass side walls were evidently far from negligible even though slip did occur.

In the present tests the shear zones spanned the full width of the channel whereas the analysis of §4.2 noted the possibility of plug-flow regions. Some preliminary tests in a wider apparatus than that described in §5.1 have shown that plug-flow regions can exist in the middle of the channel with the shear-flow regions restricted to boundary layers near the rough side walls. The widths of these shear zones appeared to be proportional to the particle diameter and were about 10 to 15 bead diameters.

7. Granular jumps

As mentioned in §2, 'granular jumps' analogous to hydraulic jumps in water can be generated by downstream channel controls or obstructions when the upstream Froude number is greater than unity. An inclined-chute test section similar to that described in §5.1 but with a smooth bottom and 25 cm high glass side walls was made for observations of granular jumps. Figure 30 (plate 4) shows the jump profiles obtained with the polystyrene beads flowing at two different upstream Froude numbers. The jump is very abrupt by comparison with the analogous hydraulic jump. The jump steepness is found to increase with upstream Froude number. Energy dissipation evidently takes place through shearing motions within the jump; since the shear stresses are so high the required dissipation can be accomplished within a relatively short distance.

† Note that this value of $\bar{\rho}$ is somewhat less than that corresponding to the values of the fractional solids content just mentioned for uniform spherical particles, $0{\cdot}58 < \nu < 0{\cdot}63$. The value of $\bar{\rho} = 0{\cdot}58$ is probably a conservative one and is based upon bulk density measurements for loose packings in containers similar in size to the experimental flow channel.

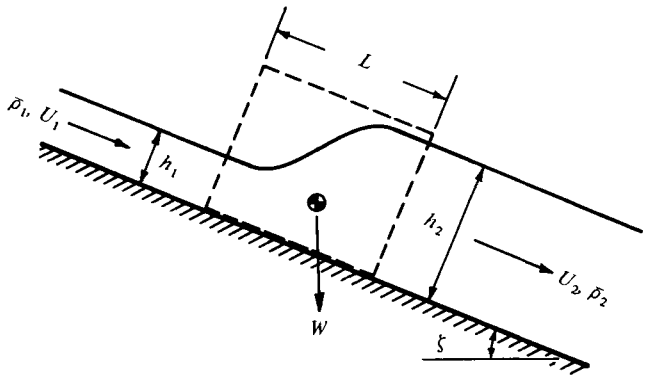

FIGURE 31. Definition sketch for granular jump.

7.1. *Theoretical analysis*

An analysis quite similar to that for the hydraulic jump may be performed to predict the depth change in the granular jump. One of the referees has drawn my attention to the work of Morrison & Richmond (1976), which contains a related but less general jump analysis than that which follows. Consider the steady two-dimensional flow of a bulk solid in an inclined channel with a granular jump as shown in figure 31. We define $\bar{\rho}_i$ and U_i respectively as the depth-averaged densities and velocities, h_i as the depths, L as the length of the granular jump, W as the weight of the material in the jump and ζ as the bed slope. The subscripts $i = 1$ and 2 refer respectively to stations upstream and downstream of the jump region. The momentum equation applied to the control volume shown yields

$$\bar{\rho}_1 U_1 h_1 w(\bar{\beta}_2 U_2 - \bar{\beta}_1 U_1) = P_1 - P_2 + W \sin\zeta - F_f \tag{7.1}$$

after making use of the continuity equation

$$\bar{\rho}_1 U_1 h_1 = \bar{\rho}_2 U_2 h_2, \tag{7.2}$$

where w is the channel width, P_1 and P_2 are the normal forces acting on sections 1 and 2, F_f is the bed and side-wall frictional force between stations 1 and 2, and the $\bar{\beta}_i$ are the Boussinesq momentum coefficients introduced to account for non-uniform velocity and density profiles. If the pressure were hydrostatic, then the normal forces P_i would be given by $\frac{1}{2}\bar{\rho}_i g h_i^2 w \cos\zeta$. Since the bulk solid is frictional it is necessary to introduce a pressure coefficient k_i analogous to the earth pressure coefficients used in soil mechanics, thus

$$P_i = \tfrac{1}{2} k_i (\bar{\rho}_i g h_i^2 w \cos\zeta). \tag{7.3}$$

We may express the weight of material in the jump as

$$W = \tfrac{1}{2}\bar{K} g w L(\bar{\rho}_1 h_1 + \bar{\rho}_2 h_2), \tag{7.3}$$

where $\bar{K}$ is a profile coefficient to account for the shape of the jump. For a trapezoidal-shaped jump of uniform density ($\bar{K} = 1{\cdot}0$), the bed and side-wall friction force may be expressed as

$$F_f = \mu_{\text{eff}} W \cos\zeta, \tag{7.5}$$

where μ_{eff} is the effective coefficient of friction and is a function of the depth-to-width ratio of the bulk solid in the channel.

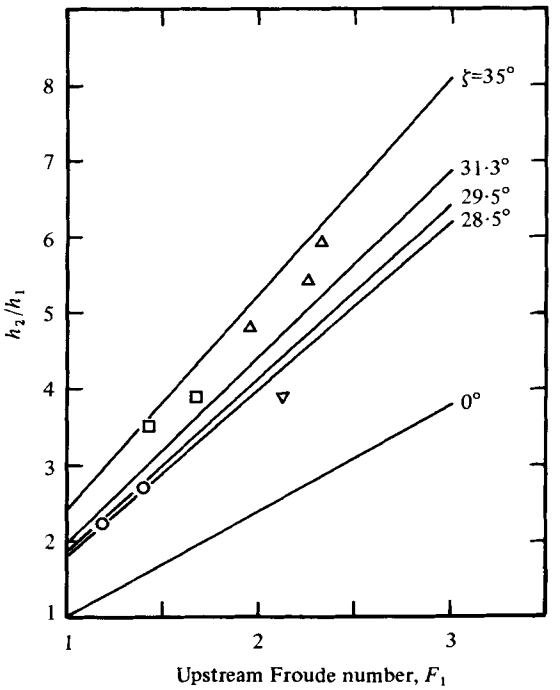

FIGURE 32. Comparison of theoretical and experimental conjugate depth ratio *vs.* upstream Froude number for granular jumps in polystyrene beads. ▽, ○, □, △, ζ = 28·5°, 29·5°, 31·3° and 35° respectively. ——, equation (7.7) for $\bar{K}L/(h_2-h_1) = 1{\cdot}0$.

Substituting (7.3)–(7.5) into (7.1) yields

$$\left(k_2\cos\zeta-\frac{\bar{K}L}{h_2}Z\right)\left(\frac{h_2}{h_1}\right)^3-\left(\frac{\bar{\rho}_1}{\bar{\rho}_2}\right)\frac{\bar{K}L}{h_2}Z\left(\frac{h_2}{h_1}\right)^2-\left(\frac{\bar{\rho}_1}{\bar{\rho}_2}\right)(2\bar{\beta}_1F_1^2+k_1\cos\zeta)\left(\frac{h_2}{h_1}\right)+2\left(\frac{\bar{\rho}_1}{\bar{\rho}_2}\right)^2\bar{\beta}_2F_1^2=0, \quad (7.6)$$

where $Z = \sin\zeta-\mu_{\text{eff}}\cos\zeta$ and $F_1 = U_1/(gh_1)^{\frac{1}{2}}$ is the upstream Froude number.

Since appropriate values for the various parameters k_i, $\bar{\beta}_i$, μ_{eff}, $\bar{K}L/h_2$, etc., are unknown *a priori*, some exploratory calculations were made to determine the effects of variations of these parameters on the relationship between h_2/h_1 and F_1 given by (7.6). Information from the tests was used as a guide in choosing ranges for the parameters. The bulk density upstream of the jump appeared in the tests to be slightly less than that downstream of the jump, hence $\bar{\rho}_1/\bar{\rho}_2 < 1$. Since the upstream flow was relatively loose and probably close to an active pressure state (in the soil-mechanics context) k_i might be expected to be close to but less than unity. The jump was generated by a downstream obstruction and hence the downstream flow was most likely in a passive state with $k_2 > 1$. While the upstream velocity profile appeared to be fairly uniform such that $\bar{\beta}_1 \simeq 1$, the downstream velocity profiles became more and more non-uniform with increasing ζ, with low velocities at the channel bottom and hence $\bar{\beta}_2 > 1$. The exploratory calculations based upon (7.6) showed that the effects of $\bar{\rho}_1/\bar{\rho}_2$ and $\bar{\beta}_2$ upon h_2/h_1 at a fixed F_1 were small and increases in k_2 and μ_{eff} each decreased h_2/h_1 at a fixed F_1. Therefore an estimate of the upper limit on h_2/h_1 may be

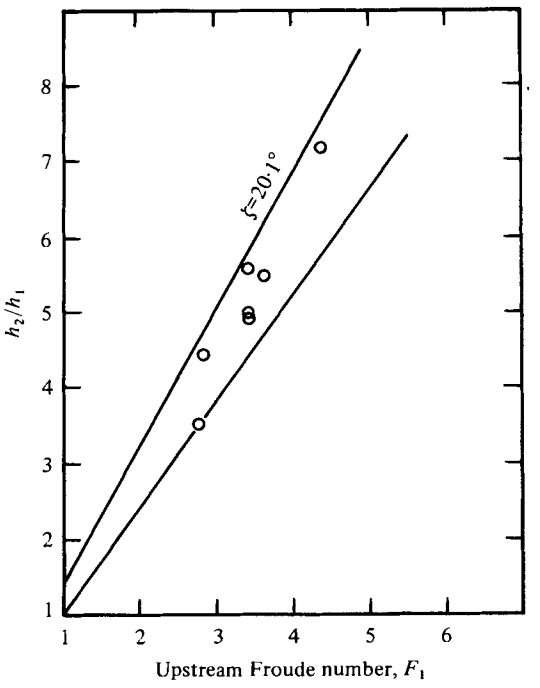

FIGURE 33. Comparison of theoretical and experimental conjugate depth ratio *vs.* upstream Froude number for granular jumps in glass beads, $\zeta = 20{\cdot}1°$. ——, equation (7.7) for $\bar{K}L/(h_2-h_1) = 1{\cdot}0$.

obtained if we take $k_i = \bar{\beta}_i = \bar{p}_1/\bar{p}_2 = 1{\cdot}0$ and $\mu_{\text{eff}} = 0$ in (7.6). Equation (7.6) then reduces to a simpler form which has the solution (Chow 1959, p. 426)

$$h_2/h_1 = \tfrac{1}{2}[(1+8G^2)^{\frac{1}{2}}-1], \tag{7.7}$$

where

$$G^2 = \frac{F_1^2}{\cos\zeta - \bar{K}L\sin\zeta/(h_2-h_1)}.$$

Comparisons of the experimental depth ratio *vs.* the upstream Froude number with the predictions of (7.7) are shown in figure 32 for the polystyrene-bead experiments and in figure 33 for the preliminary glass-bead experiments described in §2. In order to calculate the upstream Froude number from the measured depth and mass flow rate it was assumed that the bulk densities $\bar{p}_1$ were 0·55 and 1·4 g/c.c. for the polystyrene and glass beads respectively. These values of $\bar{p}_1$ are uncertain and this results in uncertainties in the values of F_1 for the experimental points. The experiments fall somewhat below the predictions of (7.7) for $\bar{K}L/(h_2-h_1) = 1$ but above those for $\zeta = 0$.

8. Concluding remarks

The foregoing work has been concerned with the flow behaviour of cohesionless bulk solids under conditions of rapid shear. A constitutive equation has been proposed which (*a*) describes a Coulomb material where the normal and shear stresses are related and (*b*) refers the stresses to the deformation rates in a nonlinear way in accordance with the experiments of Bagnold (1954). Although the present study has dealt

specifically with bulk solids flow, it also may have some bearing upon the apparent viscosity of fluidized beds. Davidson, Harrison & Guedes de Carvalho (1977) have recently suggested that fluidized-bed viscosity is caused by interparticle collisions and note the possible relevancy of Bagnold's work.

Attempts to generate experimentally the two-dimensional shear flows studied theoretically were not completely successful because of the presence of friction on the glass side walls of the flow passages. For this reason, direct comparisons of the experiments and the theoretical predictions of §4 are not appropriate. The experiments did reflect the general trends of the analyses in the shapes of both the velocity profiles and the depth profiles in the inclined chute. This lends credence to the main features, if not necessarily the detailed validity, of the proposed constitutive relation.

Further experiments concerning flow down inclined chutes much wider than those of the present paper are suggested. The primary factor hindering progress is the great difficulty of obtaining detailed experimental information during granular flow at high shear rates and low stress levels. It is encouraging that the fibre optic probes proved to be quite successful in measuring velocities of slipping flow past smooth walls or at free surfaces. However, a way to measure velocities in the interior of a flowing bulk solid without significantly disturbing the flow is still sorely needed. Measurements of local values of bulk density during flow would also be most useful.

The extreme sensitivity of the material response to very small changes in the fractional solids content ν at the higher concentrations and the complicated nature of the constitutive equation for three-dimensional flows tend to discourage the hope that one will be able to predict with confidence anything but the simplest flows.

The work reported here was supported by the National Research Council of Canada. I am indebted to C. Sciascia, S. Yap and C. C. Ko for assistance in performing some of the experimental work. A preliminary version of this paper was presented at the Euromech Colloquium 84 on *Mechanics of Granular Materials*, Warsaw, Poland, 13–16 July 1976.

REFERENCES

Allen, J. R. L. 1970 *J. Geol.* **78**, 326–351.
Aris, R. 1962 *Vectors, Tensors, and the Basic Equations of Fluid Mechanics*. Prentice-Hall.
Augenstein, D. A. & Hogg, R. 1974 *Powder Tech.* **10**, 43–49.
Bagnold, R. A. 1954 *Proc. Roy. Soc.* A **225**, 49–63.
Bagnold, R. A. 1966 *Proc. Roy. Soc.* A **295**, 219–232.
Bingham. E. C. & Wikoff, R. W. 1931 *J. Rheol.* **2**, 395–400.
Blair-Fish, P. M. & Bransby, P. L. 1973 *Trans. A.S.M.E., J. Engng Ind.* **95**, 17–26.
Bransby, P. L. & Blair-Fish, P. M. 1974 *Chem. Engng Sci.* **29**, 1061–1074.
Bransby, P. L. & Blair-Fish, P. M. 1975*a* *Powder Tech.* **11**, 273–288.
Bransby, P. L. & Blair-Fish, P. M. 1975*b* *Geotech.* **25**, 384–389.
Bridgwater, J. 1972 *A.S.M.E. Paper* no. 72-MH-21.
Brown, R. L. 1961 *Nature* **191**, 458–461.
Brown, R. L. & Richards, J. C. 1970 *Principles of Powder Mechanics*. Pergamon.
Choda, A. & Willis, A. H. 1967 *Trans. Am. Soc. Agri. Engrs* **10**, 136–138.
Chow, V. T. 1959 *Open-Channel Hydraulics*. McGraw-Hill.
Cowin, S. C. 1974*a* *Powder Tech.* **9**, 61–69.

COWIN, S. C. 1974*b* *Acta Mechanica* **20**, 41–46.

COWIN, S. C. & GOODMAN, M. A. 1976 *Z. angew. Math. Mech.* **56**, 281–286.

DAVIDSON, J. F., HARRISON, D. & GUEDES DE CARVALHO, J. R. F. 1977 *Ann. Rev. Fluid Mech.* **9**, 55–86.

DAVIDSON, J. F. & NEDDERMAN, R. M. 1973 *Trans. Inst. Chem. Engrs* **51**, 29–35.

DRUCKER, D. C. & PRAGER, W. 1952 *Quart. Appl. Math.* **10**, 157–165.

ESHELBY, J. D. 1951 *Phil. Trans. Roy. Soc.* A **244**, 87–112.

GARDNER, G. C. 1966 *Chem. Engng Sci.* **21**, 261–273.

GENIEV, G. A. 1958 *Rep. Acad. Bldg Archit. USSR.*

GOODMAN, M. A. & COWIN, S. C. 1971 *J. Fluid Mech.* **45**, 321–339.

GOODMAN, M. A. & COWIN, S. C. 1972 *Arch. Rat. Mech. Anal.* **44**, 249–266.

GREEN, A. E. & ADKINS, J. E. 1960 *Large Elastic Deformations.* Oxford: Clarendon Press.

GREEN, A. E. & RIVLIN, R. S. 1956 *Quart. Appl. Math.* **14**, 299–308.

HAGEN, G. 1852 *Berlin Monatsber. Akad. Wiss.* pp. 35–42.

JAMES, R. G. & BRANSBY, P. L. 1971 *Geotech.* **21**, 61–83.

JENIKE, A. W., JOHANSON, J. R. & CARSON, J. W. 1973 *Trans. A.S.M.E., J. Engng Ind.* **95**, 1–16.

JOSSELIN DE JONG, G. DE 1959 Ph.D. thesis, Delft University.

JOSSELIN DE JONG, G. DE 1971 *Geotech.* **21**, 155–163.

LEE, S., COWIN, S. C. & TEMPLETON, J. S. 1974 *Trans. Soc. Rheol.* **18**, 247–269.

MANDL, G. & FERNÁNDEZ LUQUE, R. 1970 *Geotech.* **20**, 277–307.

MEANS, R. E. & PARCHER, J. V. 1963 *Physical Properties of Soils.* Columbus: C. E. Merrill.

MORRISON, H. L. & RICHMOND, O. 1976 *Trans. A.S.M.E., J. Appl. Mech.* **43**, 49–53.

PARRY, R. H. G. (ed.) 1971 *Stress–Strain Behaviour of Soils. Proc. Roscoe Mem. Symp.* Leeds: G. T. Foulis.

PERRY, M. C. & JANGDA, H. A. S. 1970 *Powder Tech.* **4**, 89–96.

REYNOLDS, O. 1885 *Phil. Mag. Ser.* 5, **20**, 469–481.

RICHARDS, J. E. (ed.) 1966 *The Storage and Recovery of Particulate Solids. Inst. Chem. Engng Working Party Rep.*

RIDGWAY, K. & RUPP, R. 1970 *Chem. Process Engng* **51**, 82–85.

ROBERTS, A. W. 1969 *Trans. A.S.M.E., J. Engng Ind.* **91**, 373–381.

ROSCOE, K. H. 1970 *Geotech.* **20**, 129–170.

SAVAGE, S. B. 1965 *Brit. J. Appl. Phys.* **16**, 1885–1888.

SAVAGE, S. B. 1967 *Int. J. Mech. Sci.* **9**, 651–659.

SAVAGE, S. B. & YONG, R. N. 1970 *Int. J. Mech. Sci.* **12**, 675–693.

SCHEIDEGGER, A. E. 1975 *Physical Aspects of Natural Catastrophies.* Elsevier.

SERRIN, J. 1959 *J. Math. Mech.* **8**, 459–469.

SOKOLOVSKI, V. V. 1965 *Statics of Granular Media.* Pergamon.

SPENCER, A. J. M. 1964 *J. Mech. Phys. Solids* **12**, 337–351.

SPENCER, A. J. M. 1971 *Geotech.* **21**, 190–192.

SUZUKI, A. & TANAKA, T. 1971 *Ind. Engng Chem. Fund.* **10**, 84–91.

TAKAGI, S. 1962 *Proc. A.S.C.E.* **88** (EM3), 107–151.

TAKAHASI, K. 1937 *Geophys. Mag.* **11**, 165–175.

TERZAGHI, K. 1963 *Theoretical Soil Mechanics.* 11th printing. Wiley.

THEIMER, O. F. 1969 *Trans. A.S.M.E., J. Engng Ind.* **91**, 460–477.

TRUESDELL, C. 1974 *Ann. Rev. Fluid Mech.* **6**, 111–146.

WIEGHARDT, K. 1975 *Ann. Rev. Fluid Mech.* **7**, 89–114.

WOLF, E. G. & VON HOHENLEITEN, H. L. 1945 *Trans. A.S.M.E.* **67**, 585–599.

ZAGAYNOV, L. S. 1967 *Mech. Tverd. Tela* no. 2, pp. 188–196.

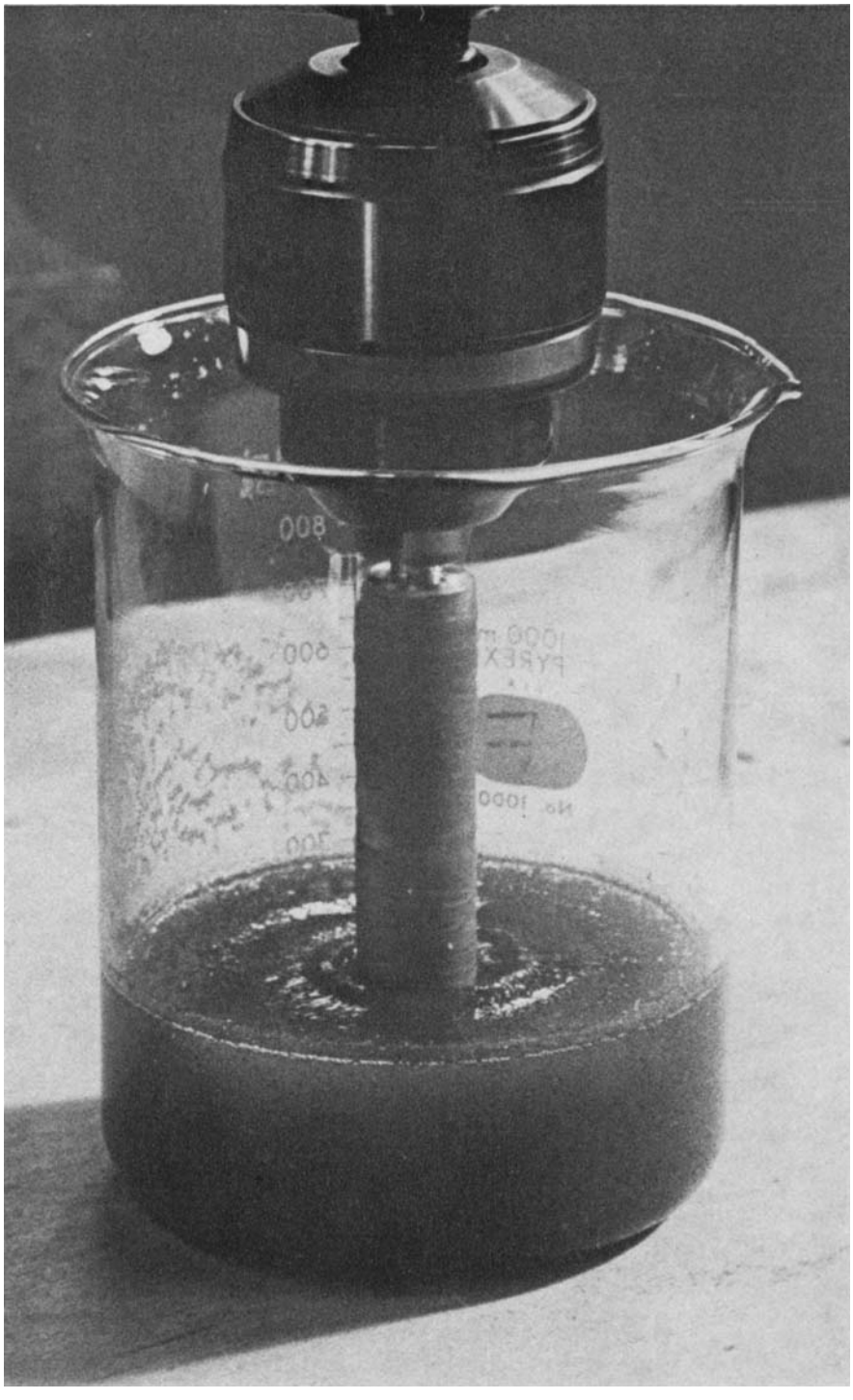

FIGURE 11. Photograph of experiment showing bump in free surface near rotating cylinder due to normal-stress effects.

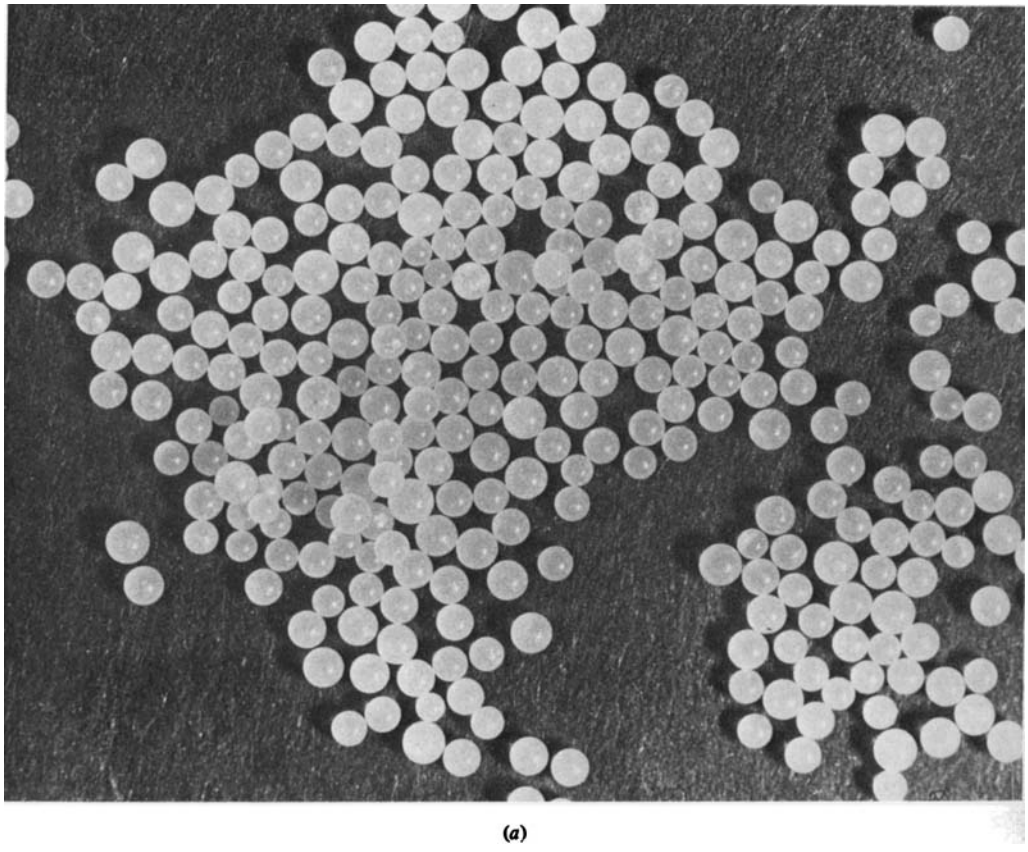

(*a*)

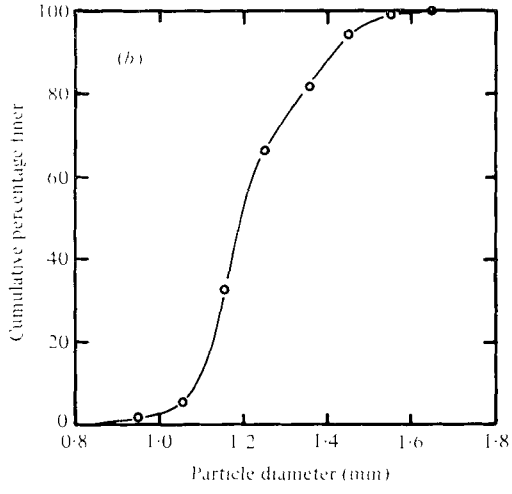

FIGURE 16. (*a*) Photograph of polystyrene beads. (*b*) Particle size distribution.

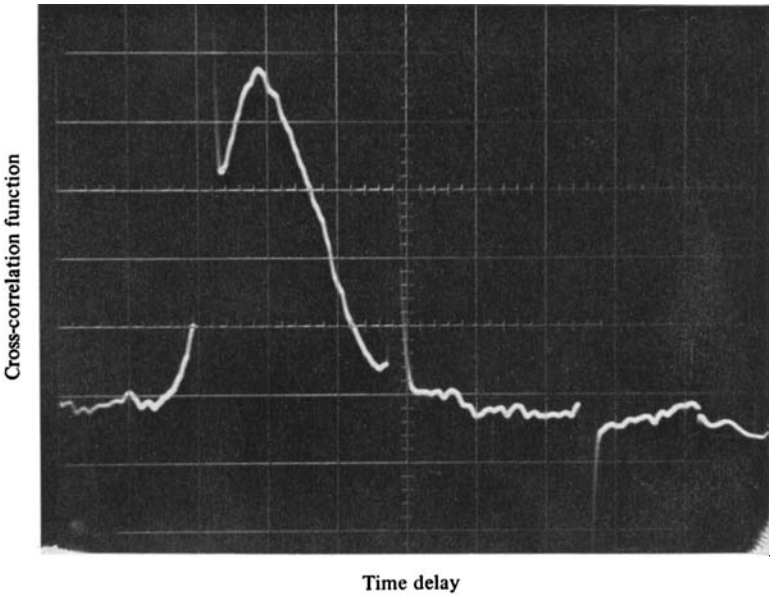

FIGURE 22. Typical oscillogram of cross-correlation function for fibre optic probes.

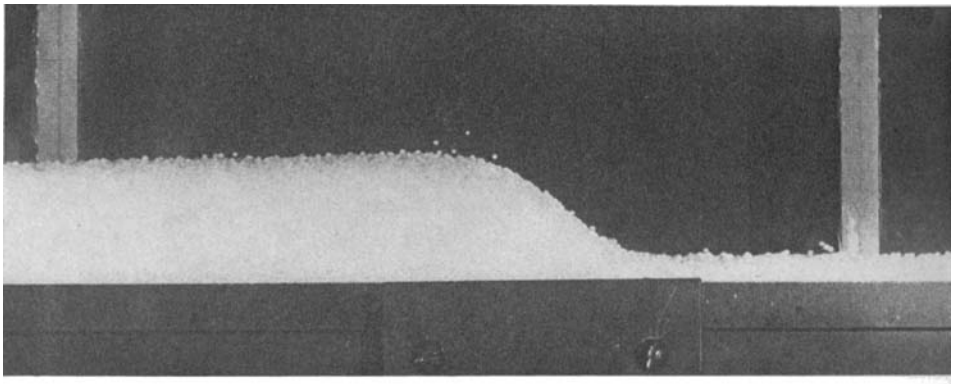

(*a*)

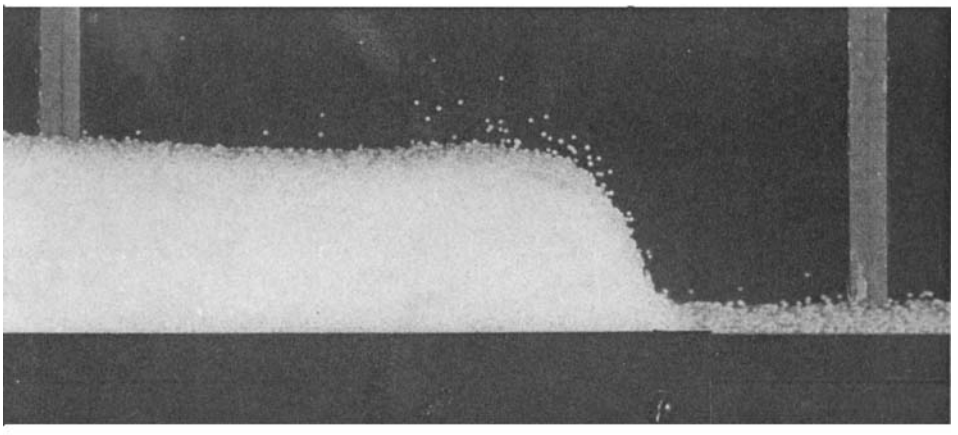

(*b*)

FIGURE 30. Granular jumps generated during flow of polystyrene beads in inclined chutes. (*a*) $\zeta = 31{\cdot}3°$, upstream Froude number $\simeq 2{\cdot}1$, conjugate depth ratio $\simeq 4{\cdot}4$. (*b*) $\zeta = 35°$, upstream Froude number $\simeq 2{\cdot}5$, conjugate depth ratio $\simeq 6$.